Investigation of Extractable Materials from Biochar

A thesis submitted in partial fulfilment

of the requirements for the degree

of

Master of Science

in Chemistry

at

The University of Waikato

by

Wenjuan (Joanna) Yang

The University of Waikato

2012

THE UNIVERSITY OF
WAIKATO
Te Whare Wānanga o Waikato

Abstract

Biochar has been used to improve soil productivity and has been a subject of discussion since 1804. However, research and development of biochar for environmental purposes on a global scale are a recent development. Due to the increase of its uses and interest in biochar as soil amendment, there is a need to understand the intrinsic chemistry of biochar to understand how this might affect its action in the soil.

In this work two principal topics were addressed:

1) Investigation of volatile organic compounds in biochar that has been derived from various biomasses and the effect of different temperatures of pyrolysis
2) Identification of some chemical structures of biochar.

GC-MS analysis identified 60 extractable organic compounds. With respect to pyrolysis temperature, GC-MS results of Green Waste chars and Sucrose chars shows that extractable organic compounds changed their proportions with differing pyrolysis temperatures. MALDI-TOF and high resolution mass spectrometry results suggested that the characteristic ions for biochar that appear in MALDI-TOF spectra with m/z values of 301,317, 413,429 and 453 are plasticizers whereas 685/ 701 are ions, $[M+Na]^+$/ $[M+K]^+$ respectively that are intrinsic to biochar.

Acknowledgements

I would like to take this opportunity to thank my supervisor Merilyn Manley-Harris for all the support and help for the past two years of study, especially with the proof-reading of my thesis and correcting all the grammar mistakes. As English is my second language, I can imagine how hard it would be, but she is always very patient, has spent a lot of time teaching me writing, and also making sure I am on the right track.

I would also like to thank the staff in the chemistry department and students who have provided help for everything that I have needed.

This project would not be completed without sample donation from Stephen Joseph (School of Materials Science and Engineering, University of New South Wales, Australia), Michael Antal (Hawai'i Natural Energy Institute), John McDonald-Wharry (University of Waikato, Chemistry Department, New Zealand), BEST Energies Australia and Marta Camps and Helen Walker (Massey University).

To Cheryl Ward the science librarian who has been very helpful to me in terms of formatting the thesis and advanced uses of Word, Endnote and Excel, thank you for your patience.

To Mum and family members:
妈妈，感谢您那无私的爱，陪伴女儿度过了 29 个春秋；您的辛劳付出,成就了女儿的今天。希望女儿今天的成绩，是对您最好的回报。
感谢我亲爱的妈妈和所有支持我的家人

Table of Contents

Additional materials are included in the CD-Rom attached at the back of the thesis

List of Figures

Introduction

Method Development

Investigation of characteristic ions of biochar

Extractives from biochar soluble in non-aqueous solvents

Studies of specialty biochars

List of Tables

Introduction

Method Development

Investigation of characteristic ions of biochar

Extractives from biochar soluble in non-aqueous solvents

Studies of specialty biochars

Abbreviations

MALDI-TOF	Matrix Assisted Laser Desorption Ionization Time-of-Flight
LDI	Laser Desorption Ionization
MS	Mass Spectrometry
GC-MS	Gas Chromatography Mass Spectrometry
NMR	Nuclear Magnetic Resonance
LC-MS	Liquid Chromatography Mass Spectrometry
ESI-MS	High Resolution Mass Spectrometry (Electrospray Ionisation)
HTT	Heat treatment temperature
FP	Fast pyrolysis
SP	Slow pyrolysis
AMU	Atomic Mass Unit
RPM	Revolutions per Minute
MW	Molecular Weight
Da	Daltons
RT	Retention time
BMC	Biochar mineral complex
MQ water	MilliQ water

Introduction

1.1 Biochar

Biochar is produced by pyrolysis[*] of biomass[†]. Biochar can be potentially applied onto agricultural fields and incorporated with the top layer of soil to improve nutrient retention and carbon storage.[1] It also has other benefits to the environment which attract scientists' interest, such as waste management, carbon sequestration and for energy production. Recently, research and development of biochar for environmental purposes have become of global interest.

1.2 Terminology

The term 'Biochar' is relatively new, emerging in conjunction with soil management and carbon sequestration issues.[2] 'Agrichar' has been used interchangeably with Biochar as well as 'Black Carbon' or 'Activated carbon'; Agrichar is a well established term that is used to describe the charred organic matter applied to soil. 'Biochar' is preferred in the case of charred organic matter that is used outside agriculture,[1] but it is also often used in agriculture as well. 'Activated carbon' is charcoal that has been activated either chemically or physically often for industrial purposes. 'Black carbon' covers a wider range of materials, for example, charcoal, biochar, graphitic black carbon and graphite.[3]

1.3 Early work on biochar

Widespread research and development of biochar for environmental purposes is recent, but the origin of the concept is ancient.[4] Biochar has been used in agriculture for thousands of years. Rich, highly fertile, dark soil was discovered by the explorer Herbert Smith in 1879, and rediscovered by a Dutch soil scientist Wim Sombroek in the 1950s in the Amazon rain forest.[5]

[*] A thermal decomposition process in the absence of oxygen

[†] Biomass - term used to describe materials derived from plants or animals often used to describe agricultural or forestry waste

These dark soils known as Terra Preta, have supported the agricultural needs of the Amazonians for centuries and only exist in inhabited areas which indicates that humans are responsible for their creation. Analyses of the Terra Preta found a high concentration of charcoal and activated carbon to be the major ingredients together with organic matter, such as plant and animal remains (manure, blood and bones).[6]

In 1851, Trimble described the effect of charcoal dust in increasing and quickening vegetation; Retan and Tryon in the early 20th century investigated the effects of charcoal on seedling growth and soil chemistry,[7, 8] and suggested that charcoal has potential in fertilizing the soil and thus increasing crop growth.

1.4 Charcoal production and applications

Charcoal is well known and has an ancient production history for use in production of heat and energy, predominantly in cooking. Several techniques have been developed for charcoal production based on traditional kilns to improve the productivity and quality. Because of the non-renewable nature of fossil fuel and shortage of wood supply for the production of charcoal, the pyrolysis of biomass has become a platform for energy production and bio-renewable resources.[9]

1.4.1 Traditional charcoal production and its uses

There is an extensive history in manufacture and use of charcoal since 38000 years ago.[10] It was initially produced in open fires, either forest fires or camp fires, and thus was available for early mankind to use in cave paintings. The presence of microscopic charcoal in lake sediments, peat, and soil provides evidence of fire occurrence in the past.[11]

The charcoal industry was established around 1100 BC with the fuel playing a significant role in daily life. The earliest charcoal kilns consisted of a pit or mound. Both of the techniques involved covering the biomass; wood in most cases, with earth. Earth was used for the purpose of controlling oxygen (O_2) availability and heat loss during carbonization. These kilns produce relatively low charcoal yields of inconsistent quality and released poisonous gases. While these

simple and low cost kilns persist to this day in many developing and undeveloped countries, various kinds of kilns have been developed to improve the yield and quality of charcoal.[12]

The most commonly used kilns in industry today include the Missouri kiln and the Brazilian Beehive kiln. The Missouri kiln yields charcoal at a range between 25%-33% oven dry weight, operates on a cycle which takes about 28 days of which the cooling process takes a minimum 21days and that can be longer with warm weather. The Brazilian Beehive kiln, operating on a 8 day cycle has charcoal yields up to 35%.[13, 14] The Food and Agriculture Organization of the United Nations statistics data (FAOSTAT) showed that globally about 47 million metric tonnes of wood charcoal were produced in 2009, and this was often used for chemical applications, barbeques or steel production.[15]

1.4.2 Production of biochar

The thermal decomposition of biomass occurs in a closed, O_2-deprived condition called pyrolysis. The products are liquid, biochar and gases which vary in proportion depending on the composition of the biomass and the conditions under which pyrolysis occurs.[16] For example, the distribution of products can be altered by changing particle size and reaction parameters such as reaction time and gas flow rate through the fluidized bed. A low temperature (<700˚C) pyrolysis, obtains mainly char products, whereas high temperature (>700˚C) pyrolysis is also known as gasification, syngas is the preferential product (**Table 1. 1**).

There are two main pyrolysis systems ‘slow’ pyrolysis (SP, 1-20 ℃/min), and ‘fast’ pyrolysis (FP, rapid heating rate which is able to finish the process in seconds). The majority of charcoal-making technologies are SP, the system can be optimized to produce substantially more biochar. This biochar is beneficial for agronomic, as well as carbon sequestration purposes and can influence nitrous oxide (N_2O) emission.[17]

Table 1. 1 Typical product yields (dry basis) for different modes of pyrolysis, adapted from Bridgwater (2007)[18]

Mode	Conditions	Liquid (%)	Char (%)	Gas (%)
Fast	Moderate temperature ~500˚C, short hot vapour residence time ~1 sec.	75	2	13
Moderate	Moderate temperature ~500˚C, moderate hot vapour residence time 10-20 sec.	50	20	30
Slow	Low temperature ~400˚C, very long solids residence time	30	35	35
Gasfication	High temperature ~750˚C long vapour residence time	5	10	85

Fast pyrolysis (FP) heats biomass rapidly and extract vapours for the preferential production of bio-oil over gas and biochar.[19] In addition, the biochar produced by FP is usually very fine powders, [20] and has different properties from SP biochar, which it is believed impact differently on soil fertility.[21] Bruun (2011)[22] showed that FP biochar improves the water holding capacity by 32% on sandy loam soil, and is able to immobilize a reasonable amount of nitrogen (N) in soil. Nevertheless, the effects seem like a transient phenomenon, thus more field trials are needed in order to verify potential benefits for agronomic uses.

There are some advanced technologies developed for biochar manufacture including: drum pyrolysers, rotary kilns, screw pyrolysers, the Flash Carbonizer™, fast pyrolysis reactors, gasifiers, hydrothermal processing reactors and wood gas stoves that help to improve energy efficiency, reduce pollution emissions and increase feedstock flexibility, thereby improving biochar production and utilization.[1] However, there is very little available literature on the yields and properties of biochar related to agronomic or environmental management applications.

1.5 Biomass-composition and thermal decomposition

Biomass is a term that is used to describe a wide variety of materials including crop and forest residues (e.g. sawdust, grain crops and nut shells) or organic wastes (e.g. green waste and animal manures).[23] Globally, about 11% of primary energy is provided by plant material. The main constituents of plants are cellulose, hemicellulose, and lignin with small amounts of extractives and inorganic minerals.[1, 24] These components can vary between biomass or even within a species depending on the location, time of collection and environmental conditions.[25- 28]

1.5.1 Cellulose

Cellulose, is a linear homo-polysaccharide comprised of several hundred or thousands of D-glucose units linked by β-(1 →4)-glycosidic linkages.[29] It is the largest component of biomass, and the most common organic compound on Earth. Every year, there are about 100 billion tonnes produced by plants. In plant cell walls, many parallel cellulose molecules are stacked on top of each other to form an aggregated micro-fibril crystallite resulting from hydrogen bonding and Van der Waal's forces. This gives cellulose high tensile strength and more resistance to thermal decomposition than hemicellulose.

1.5.2 Hemicellulose

Hemicellulose is a group of hetero-polysaccharides existing along with cellulose in plant cell walls. The hetero-polysaccharides contain D-glucose, D-mannose, D-xylose, D-galactose, D-arabinose and small amounts of L-sugar monomers such as L-arabinose and L-rhamnose, uronic acids and galacturonic acid.[30]
Because of the low degree of polymerization, of only 100-200 and the random and amorphous branched structure, hemicellulose has lower chemical and thermal stability than cellulose and hemicelluloses can be easily hydrolysed by acid or base.[30, 31] The composition of hemicelluloses differs between hardwood and softwood, as more mannose, galactose units and less xylose unit and acetylated hydroxyl groups are found in softwood compared to hardwood.

1.5.3 Lignin

Lignin is a complex three dimensional aromatic structure based on phenylpropane units.[32] The three construction monomers are coniferyl alcohol, sinapyl alcohol and coumaryl alcohol (**Figure 1. 1**).

In hardwood, guaiacyl-syringyl lignin is a co-polymer of coniferyl and sinapyl alcohols whereas in softwoods it is predominantly guaiacyl; a higher fraction of coniferyl alcohol is found in softwood.[33] Lignin is located mainly on the exterior of micro-fibrils, and also covalently bonded to hemicelluloses, and thus imparts rigidity to the cell wall. Lignin affects the internal transformation of water, nutrients, and metabolites and lignified tissues help resist attack by microorganisms.[34] Because it is covalently bonded, lignin is not readily depolymerised.

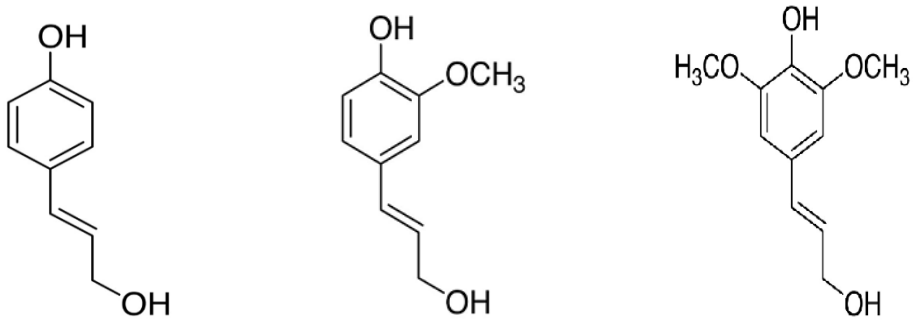

p-coumaryl alcohol Coniferyl alcohol Sinapyl alcohol

Figure 1. 1 Three phenyl-propanoid precursors of lignin[35]

1.5.4 Extractives and inorganic contents

Extractives are organic compounds from biomass that are not part of cellulose, hemicelluloses or lignin structure. These organic compounds can be extracted by water or organic solvents depending on their solubility. However, the extractives found vary with biomass used. ASTM1960-95[36] is the standard test method for determination of extractives in biomass. The possible extractives includes resins, fats and fatty acids, phenolics and phytosterols, carbohydrates and inorganic contents, these contribute to gaseous emission during pyrolysis. These extractives are believed to have no significant effect on charcoal yields.[1]

The nutrient inorganic minerals from biomass are nitrogen (N), phosphorus (P) and potassium (K). The inorganic contents from biomass are the residue remaining after dry oxidation at high temperature and are known as ash. Normally ash is comprised of alkali and alkaline chlorides, sulphates, carbonates and complex silicates.[37] There are numerous approaches developed to reduce the amount of inorganic minerals in biomass prior to pyrolysis.[37, 96]

1.5.5 Thermal decomposition of cellulose, hemicelluloses and lignin

The decomposition of cellulose, hemicelluloses and lignin is temperature and heating rate dependent.[38, 39]

A thermo-gravimetric analyser (TGA) was used to investigate the thermal degradation of these three constituents of biomass by Yang e*t al.* (2007), [40] operating with a constant heating rate at 10 ˚C/min and 120 ml/min of N_2. Hemicelluloses started to decompose at 220 ˚C and this was completed by 315 ˚C whereas cellulose does not begin to decompose until 315 ˚C. Lignin is the first to decompose at lower temperature of 160 ˚C compared to others, although the process is very slow and steady, continuously to 900 ˚C. The thermal decomposition products of hemicelluloses, cellulose and lignin pyrolysis are shown in **Table 1. 2**.

Table 1. 2 Pyrolysis products of cellulose, hemicellulose and lignin

	Products	Reference
Cellulose	Mostly solid C (biochar), CO_2 and water; small quantities of CO and CH_4	Antal *et al.* 2003[10]
Hemicellulose	Non-condensable gases[a], carboxylic acids, aldehydes, alkanes, ethers and water	Rutherford *et al*. 2004[41]
Lignin	Non-condensable gases[b], condensable vapours and liquid aerosols[c], and biochar	Mohan *et al.* 2006[19]

[a] *Non-condensable gases obtained from cellulose thermal decomposition: CO, CO_2, H_2 and CH_4*[10]

[b] *Non-condensable gases obtained from thermal decomposition of hemicellulose: CO, CH_4 and C_2H_4*[41]

[c] *Condensable vapours and liquid aerosols are as pyroligneous acid and insoluble tar. The pyroligneous acid is principally methanol and acetic acid in water; insoluble tar contains phenolic compounds derived from cleavage of ether and C-C bonds*[19]

1.6 The structure of biochar

1.6.1 The chemical structure of biochar

The structure of charcoal is different from other highly carbonaceous materials such as diamond, graphite and fullerene the most common allotropes of carbon. For example charcoal does not show the typical XRD signal of graphite. The carbon in charcoal and coal is described as amorphous. An early X-ray diffraction (XRD) experiment carried out by Randall[42] suggested that amorphous carbon is actually microcrystalline graphite. This idea was supported by a study of Ceylon natural graphite performed by Walker *et al.*[43] who showed that the characteristic graphitic peak in the XRD spectrum decreased rapidly as the sample was ground more finely. In the fine ground graphite carbon was shown to be turbostratically* arranged.[44]

The carbon product produced from pyrolysis of biomass can be divided into two distinct classes, non-graphitic carbon and graphitic carbon as was first

* Turbostratic - individual graphite planes are not aligned.

demonstrated by Franklin in 1951.[45] Material that has turbostratic structure is described as non-graphitic carbon.[46] During the process of pyrolysis, some of the non-graphitic carbons start to change into graphitic carbons as temperature increases, and eventually all may be converted into graphite when heated up to 3500˚C (**Figure 1. 2**). However, this change depends on the feedstock of biomass; graphitization can also occur at heat treatment temperatures (HTT) under 2000˚C in some cases[47] and some may not graphitize at all.

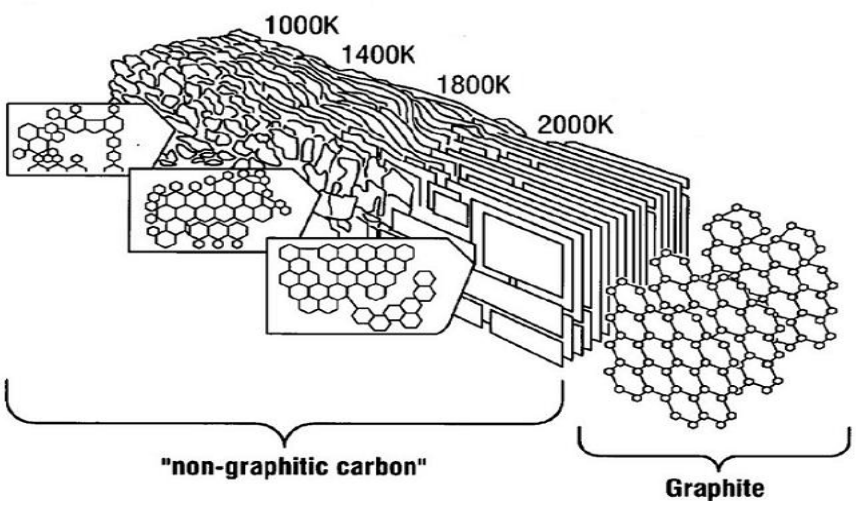

Figure 1. 2 Structure of non-graphitic and graphitic carbon, reference from[48]

Transmission Electron Microscopy (TEM) and High Resolution Electron Microscopy (HREM) have been used to study carbons, and some have reported that the non-graphitic carbons contain graphite and diamond like structures.[49, 50] In the study carried out by Harris[51] using HREM it was suggested that the microstructure observed in non-graphitic carbon might actually be fullerene-like structures.

The major difference between the two types of carbon obtained from the pyrolysis process is the orientation of the individual units evolved. In non-graphitic carbon, the individual units are randomly distributed with extensive cross-linkages in between, which prevent alignment in parallel. To prevent graphitization at high temperatures, these cross links have to be extremely strong. Carbohydrate based materials are classified as non-graphititizing.[45] In the case of graphitic carbon; the individual units are nicely aligned in the axial axis with less amounts and weaker cross linkages. Therefore the crystalline graphite formation occurs easily with the

latter type of carbon. High C/H ratios in the biomass also enhance the formation of crystalline graphite.[52]

There is limited information about the chemical structure of biochar. The earliest studies were based on the interest of developing activated carbon for the purposes of separation and purification for gases, liquids and solids.[53] Activated carbons contain high internal surface area and microporosity. Due to the char precursors used in their formation activated carbons shared similarities with biochar; hence the literature on activated carbon can be relevant to biochar.[54, 55] From these studies it is known that the physical properties of biochar depend upon the biomass utilized and also the system in which they are made. Since the feedstock of biomass can be from a wide variety of materials, the initial structure of the biomass is reflected in the biochar product and thus would greatly impact on its physical properties.[56, 57] The chemical composition of the feedstock also influences the physical nature of the biochar; the proportions of the major components (cellulose, hemicellulose and lignin) of biomass can vary. The decomposition of these components is temperature and heating rate related[38, 39] (Section 1.5.5). Lua *et al.* (2004)[54] evaluated the effect of temperature on the biochar structure and suggested that the heating rate also has a significant effect on the structure.

1.6.2 Effect of pyrolysis on structural complexity

It is known that the pyrolysis conditions affect the final structure of biochar.[10, 58, 54, 20] Factors include heating rate, HTT, long retention time and ash content. These factors in the carbonization process contribute to the loss of surface area and porosity in biochar product. Numerous studies have been performed, in which the severe loss of structural complexity of biochar under certain conditions was reported.

In 1993, Rodriguez-Misaro *et al*.[59] carried out a study on the effect of temperature on the microporous structure of biochar made from eucalyptus kraft lignin during pyrolysis and characterization of the biochar product. The high inorganic content (ash) in the biomass was found to affect the melting and swelling during the pyrolysis process. Pre-treatment by washing the starting materials with weak acid

to remove the ash content prevented the loss of structural complexity in biochar.[59] However if the starting material contains low ash content this has also been reported to cause loss of structural complexity in biochar such as hazelnut shell.[60]

Biagini and Tognotti[58] characterized the structure of biochar which was made at high heating rates; they suggested that the loss of structure can be explained by the melting of the cell structure and plastic transformations. The heating rate has been reported to be accountable for the loss of structure of biochar. Cetin *et al.* (2004)[61] studied the effect of heating rates on biochar structure. With slow heating rate (20 ˚C/sec), the volatiles released are able to escape due to the porosity of the starting materials without much alteration on biochar morphology; whereas with fast heating rate (500 ˚C/sec), the melting of cell structure is caused by rapid evolution of volatiles which cannot readily escape.[61] It was noted that this phenomenon is more prominent for materials that contain more volatile material.[58] It seems likely that the rate of heating may also affect the total mass of extractives remaining in the biochar.

Lua *et al.* (2004)[54] carried out a study on the effects of pyrolysis conditions on the physical properties of activated carbon made from pistachio nut shells and found that the BET surface area decreased progressively due to the decomposition and softening of some volatiles when increasing HTT from 500-800 ˚C. The same observation was also reported on biochar made from pine by Brown *et al.* (2006)[62] and biochar made from corncob by Bourke.[63]

Increasing retention time in the carbonization process can also influence loss of structural complexity.[64] The biochar made from oil palm stone, at 900˚C, showed decrease in surface area with increase in retention time. This was attributed to the shrinkage and realignment in biochar structure. The authors found that oil palm stone pyrolyzed at 800˚C with three hours retention time resulted in maximum surface area.

1.6.3 MALDI-TOF-MS studies on carbonaceous materials

For studies on biochar structure, structure analysis techniques are commonly used such as X-ray diffraction and scanning electron microscopy. MALDI-TOF-MS can also be used.

In matrix assisted laser desorption ionization (MALDI), a matrix is added to the sample to help ionization taken place. The matrix molecule is commonly a small aromatic compound, and easily excited by the laser pulse (UV light). The energy absorbed by the matrix is then transferred onto the analyte to assist the ionization. Because the ionization process prevents analyte molecules being thermally decomposed, it is referred to as soft ionization. Singly charged ions are generally produced under this ionization process.

In LDI the matrix is omitted because the substrate can absorb energy at the correct wavelength; for biocarbons and other carbons a matrix is not required and so the technique is called LDI. MALDI-TOF mass spectrometry has been utilized in the study of various carbon materials with or without matrix by several researchers. The compound 7, 7, 8, 8-tetracyanoquinodimethane (TCNQ) has been reported by Przybilla *et al.* (2000)[65] and Edwards *et al.* (2003)[66] as a successful matrix for analyzing insoluble carbonaceous materials using a non-solvent sample preparation technique. This technique, developed as an alternative to co-crystallization, involves the sample and matrix being ground and mixed homogenously before being compressed on the MALDI target and provides a reproducible mass spectrum with high resolution. The giant polycyclic aromatic hydrocarbons (PAHs) with molecular weight that exceeded the LDI detection limit (~ 2000)[†] were able to be characterized,[65] and also accurate spectra for petroleum pitches with the observation of trimers and tetramers (carbon clusters) were reported[66] using this technique.

In the LDI study carried out by Sedo *et al.* (2006) [67], carbon clusters were also observed on graphite, glassy carbon, carbon nanotube and synthetic diamond, the formation of one set of singly charged carbon clusters was observed in linear negative mode, C_n^- with n =1-19. In positive mode two sets were observed, the

[†] MALDI, which was used in reference 65 has no strict upper mass limit.

first set of carbon clusters, C_n^+ (with n = 1-31) was observed after exceeding the initial threshold laser power which differed between materials. Another set of heavy odd numbered positively charged carbon clusters were observed after exceeding the second threshold laser power of these materials.

MALDI-TOF mass spectrometry was explored by Bourke[63] for studying the atomic structure of biochar made from corncob. The analyses were carried out in linear mode with both polarity of ions and with no matrix. He also observed the set of small positive charged carbon clusters and negative charged clusters reported by Sedo *et al.* (2006),[67] but the second set of large carbon clusters were not observed in corncob biochar. Instead a series of discrete ions were observed with low laser power, with *m/z* values of 317, 429, 453, 465, 685 and 701. These ions were reported as the characteristic peaks of biochar and a model structure of biochar was also proposed which incorporated some of these. The MALDI spectrum of corncob biochar showed no ion of *m/z* 720 indicative of fullerene, thus this biochar contained no fullerene structures.

1.7 Research objectives

The two principal goals of this research:

- Investigate characteristic ions such as *m/z* 701. This will include:
  1) Finding a solvent which gives reliable LDI-TOF spectrum and is suitable for other conventional analytical techniques.
  2) Determining the operational mode for LDI-TOF analysis
  3) Developing a method that will allow extraction of *m/z* 701 into the solvent layer for the purpose of structural elucidation

- Investigate extractable materials (entrained volatiles) from biochar
  1) Analyzing various biochars that were made from the same biomass at different temperatures or from different biomass.
  2) Extraction solvents and silylation reagent determination
  3) Initiating a database from purchased standards

Experimental

2.1 Materials

Glassware used in this study was acid washed in 2M HNO_3

Chemicals

A fullerene (C_{60}) standard (99.5%) was purchased from MER Cooperation Tucson, Tri-Sil HTP was purchased from Thermo Scientific and sugar standards are purchased from Sigma-Aldrich.

Solvents

Solvents used were analytical grade purchased from Ajax Finechem Pty. Ltd. or HPLC grade from Scharlau.

Type 1 water (distilled and deionised) was obtained using a Barnstead system (17 megaohms).

Biochars

All samples were ground with a mortar and pestle before analysis unless specified. Biochar samples were kindly supplied by Stephen Joseph[*] (BMC 3/09, 5/09, 6/09 and 7/09; Acacia saligna biochar 400 ℃; Eucalyptus sawdust 550 ℃, 600 ℃; Chicken litter 450 ℃; Paper sludge 550 ℃); Michael Antal[†] (Hawai'i biochar 070706, Coconut shell-commercial); John McDonald-Wharry[‡] (Sucrose biochar 400 ℃, 550 ℃, 700 ℃) and Pacific Pyrolysis[§] (Green-waste biochar 350 ℃, 450 ℃, 550 ℃)

[*] University of New South Wales, Sydney, Australia

[†] Hawai'i Natural Energy Institute, University of Hawai'i, Honolulu, HI, USA

[‡] University of Waikato, New Zealand

[§] BEST Energies Australia Pty Ltd

2.2 Laser Desorption/Ionization Time-Of-Flight Mass Spectrometry (LDI-TOF MS)

Positive ion mass spectra were acquired on an Autoflex II MALDI TOF/TOF™ Proteomics Analyzer (Bruker Daltonics), with a nitrogen laser (337 nm) operating at a frequency of 10 Hz in reflector mode. Generated ions were accelerated at 20 kV and the detector voltage was 1.6 kV. Mass spectra were obtained by accumulation of at least 210 laser shots at a laser power of 45%.

Standard Calibration

A fullerene (C_{60}) standard was used for calibration of mass spectrometer prior to measurement. Fullerene (~2 mg) was suspended in toluene (1 mL). The solution was spotted in the centre of four sample cells of the target plate (see **Figure 2. 1**) and analyzed as a sample. The *m/z* value of fullerene analyzed (*m/z* 720.3) was adjusted to fullerite- C_{60} (*m/z* 720) calibration for this instrument. This is called external calibration. Due to the condition of the target used, calibration was carried out at the four corners of the target.

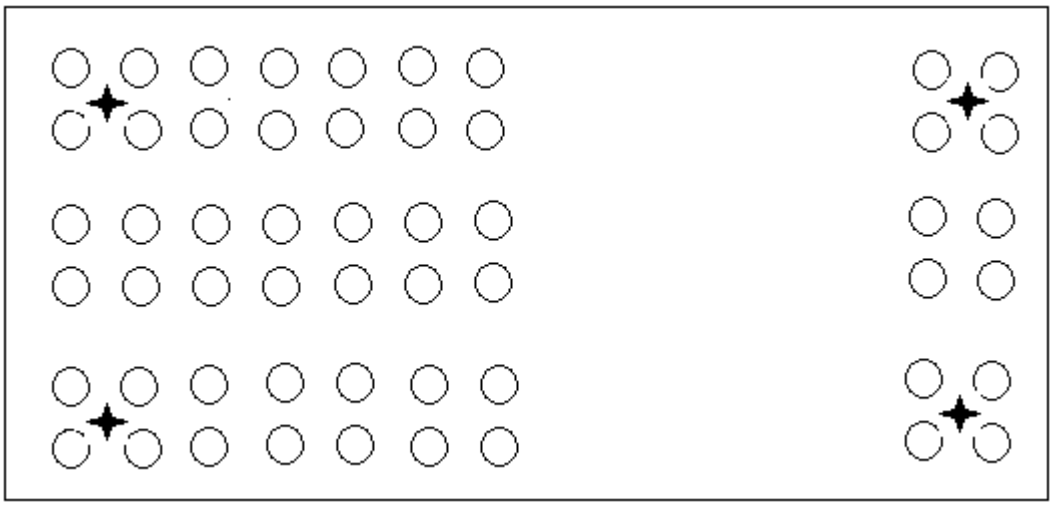

Figure 2. 1 Schematic of a polished steel MALDI target, four stars at the corners indicate the fullerene (C_{60}) spots.

2.3 Electrospray ionization Time-Of-Flight mass spectrometry (ESI-TOF or MicrOTOF)

High resolution spectra were obtained from a Bruker Daltonics electro spray ionization (ESI) mass spectrometer. The mass spectrometer was equipped with a TOF analyzer which provided an accurate measurement for *m/z* values up to four decimal places. The analysis was undertaken in positive ion mode only.

Instrument Calibration

Sodium formate solution was used as calibration standard for ion *m/z* 701; it covers the MS range up to 1700 amu in positive mode. To ensure that accurate mass measurements were obtained, at least 30 minutes stabilization was required. Separate syringes and delivery tubes were used for calibration standards and sample to avoid cross-contamination. This calibration was carried out as an internal calibration by acquiring approximately 0.5 min with sodium formate solution, and then pausing the acquisition and replacing the standard with a sample delivery tube for further acquisition.

2.4 Inductively Coupled Mass Spectrometry with Laser ablation and solution introduction

2.4.1 Laser ablation inductively coupled mass spectrometry (LA-ICP-MS)

LA-ICP-MS was carried out on a New Wave UP-213 laser ablation system equipped with a Nd:YAG 213 nm laser controlled by a laser ablation software. The laser was connected to a PerkinElmer SCIEX ELAN®DRC II inductively coupled mass spectrometer with a quadruple mass spectrometer (Concord, Ontario, Canada). The ICP was operated on ELAN software, version 3.3. The instrument parameters used are shown in **Table 2. 1**

Table 2. 1 Parameters for ICP-MS for laser ablation

Parameter	Value	Unit
He as carrier gas through cell	1	$mLmin^{-1}$
Ar as carrier gas after cell	0.6	$Lmin^{-1}$
Plasma gas	15	$Lmin^{-1}$
Auxiliary gas	1.2	$Lmin^{-1}$
Dwell time per AMU	10	ms
RF value	1350	W

Instrument Calibration

Liquid calibration solutions used were ELAN DRC Setup/Stablility/Masscal (10 ppb) and dual detector calibration solution. The dual detector solution was made by mixing 50 mL Ca (1000 ppm), 17 mL Fe (1000 ppm) and 1 mL Merck XXI in a volumetric flask (1 L) with 2% nitric acid. 15 mL of this solution was made up to 50 mL in a Falcon™ tube with Type **1** water.[68] A series of liquid calibration solutions were run in a specific order to ensure optimum performance of the ICP-MS.

Solid calibration material used was a standard reference material (NIST 612), a glass obtained from National Institute of Standards and Technology. NIST 612 was ablated for 2 minutes as a raster, with a 50 μm spot and 90% laser power.

2.4.2 ICP-MS analysis of digest

Digested biochar samples were analyzed via ICP-MS (PerkinElmer SCIEX, ELAN®II) utilizing a concentric Teflon® nebulizer (PFA-ST) with a baffled quartz cyclonic spray chamber. A Cetac auto-sampler (ASX-520) was connected to the ICP-MS that also operated under ELAN software, version 3.3. The parameters used are shown in **Table 2. 2**.

Table 2. 2 ICP-MS parameters for solutions

Parameter	Value	Unit
Ar gas flow:		
Nebulizer	0.84	$Lmin^{-1}$
Plasma gas	15	$Lmin^{-1}$
Auxiliary gas	1.2	$Lmin^{-1}$
Sample uptake rate	1	$mLmin^{-1}$
RF value	1100	W
Sweeps/reading	5	-
Reading/replicate	1	-
Replicates	3	-
Lens voltage	9	V

Instrument Calibration

Samples were analyzed together with internal standard, external standards and quality control standards **(Table 2. 3**) to ensure the instrument performance. Both types of standards are mixed with 2% nitric acid. Internal standard is added online, 50:50 standard: sample through a mixing block.

Table 2. 3 List of standards used in ICP-MS analysis

Internal standards +2% HNO_3	External standards +2% HNO_3	QC samples
2 ppm Sc	Merck XXI 50 ppb	River Water QC
2 ppm Ga	Merck IV 50 ppb	Merck XXI
200 ppb Te	Merck IV 1000 ppb	Merck IV 1000 ppb
40 ppb Rh	Merck P 5000 ppb	Merck P
20 ppb Lu		

2.5 Nuclear Magnetic Resonance (NMR)

NMR measurements were carried out on both Bruker Avance DRX-400 and DRX-300 spectrometers which were controlled by Topspin 3.0 and Topspin 2.1 software respectively.

2.6 Liquid Chromatography Mass spectrometry (LC-MS)

LC-MS measurements were performed on a Dionex Ultimate 3000 LC system connected to a Bruker amaZon X Ion Trap mass spectrometer. The mass spectrometer was operated with an atmospheric-pressure chemical ionization (APCI) source.

The sample extract was introduced via a Prodigy ODS C_{18} column (Phenomenex, 150 x 2.1 mm, 5 μm) with mobile phase MeOH in MQ water (80%, mixed by Ultimate 3600 pump) using isocratic conditions.

2.7 Gas Chromatography-Mass Spectrometry (GC-MS)

GC-MS was carried out using a cross-linked 5% phenyl-methylpolysiloxane column, installed in a Hewlett-Packard 6890 series gas chromatograph directly interfaced with an HP5973 mass selective detector. The sample (5 μL) analysis was carried out with a split injector, in full scan mode, using the temperature program with oven temperature at 55 ˚C held for 2 min, ramped to 300 ˚C at 5 ˚C/min and held for another 30 min.

Sample sequence and washes

A sample sequence and additional wash cycles were designed to prevent cross-contamination occurring between samples. A solvent blank was analyzed before and after the sequence, and a duplicate analysis of the first sample of each run was also performed. The injection syringe was washed with solvent five times before and after each injection.

Instrument calibration

The instrument calibration was carried out daily before any analysis. Autotune was performed to calibrate and target tune specific ions from, perfluorotributylamine (PFTBA). In order to avoid any leakage, air and water checks were also performed.

2.8 Extraction Methods

2.8.1 LDI-TOF spectrometry

Rapid method

Acetone (100 μL) was added to ~2 mg of finely ground biochar, mixed with a vortex mixer, and centrifuged (~1 min for each process). Aliquots (~0.5 μL) of liquid containing suspended fine particles or clear supernatant were deposited onto a polished steel Bruker target plate (MTP 384) and dried before analysis. The supernatant gave access to material that has entered into the solution. No matrix was used in either case, thus this is LDI-TOF, which indicates that there are molecules with a high degree of unsaturation and capable of absorbing laser radiation to ionize in biochar.

Liquid and solid samples of biochar were analyzed on a separate target to prevent cross-contamination.

Extended method (Hawai'i biochar only)

(a) Ground Hawai'i biochar (070706, ~10 g) stirred with acetone (50 mL) under reflux at RT (5 hr) and then left to stand (~2 hr) before the supernatant was deposited onto the target plate, and analyzed as described above for ion *m/z* 701. **(b)** Same procedure as in (**a**) but with ethyl acetate (50 mL) and a small amount of dimethyl sulfoxide (DMSO, ~100 μL) was used for extracting ion *m/z* 429. The extract obtained from (**a**) was also used for MicrOTOF, GC-MS and NMR analyses, whereas the extract from (**b**) was analyzed on MicrOTOF in addition to LDI-TOF.

2.8.2 MicrOTOF spectrometry

Aliquots of the organic extracts obtained from the extended method were diluted with MeOH (1 mL) in a micro-centrifuge vial (2 mL) to give a concentration of ~ 0.1 mg/mL solution. The solution was mixed by a vortex and centrifuged before introduction into the spectrometer via a syringe pump set at 180 μL/h.

2.8.3 ICP-MS

LA-ICP-MS

The biochar with the biggest particle size (BMC 07/09) was analyzed with 50% laser power. Four fragments of one biochar particle were placed on a microscope slide (two fragments with the inside exposed and two with the outside exposed) using a double sided tape to hold sample fragments in place during ablation.

Digestion

This method was adapted from US EPA standard Method 200.2. Ground biochar samples (0.5 g) were weighed into separate Falcon^{TM} tubes (50 mL), HNO3 (2 mL, 1:2 v/v) and HCl (5 mL, 1:5 v/v) were added and heated in a heating block (2 hr, 75 ℃). The entire sample was decanted into a volumetric flask (100 mL) and made up with Type 1 water, and then let stand overnight. This solution was further diluted (1:5 v/v) to adjust the chloride concentration to be within range for analysis.

2.8.4 NMR

The organic extract of Hawai'i biochar obtained using extended method **(a)** as described in Section 2.6 was investigated. The supernatant of this extract was evaporated to dryness under a stream of N_2 gas and re-dissolved in deuterated acetone-d_6 $(CD_3)_2CO$. This solution was centrifuged and transferred into a NMR tube for analyses with 400 MHz NMR spectrometer. Fine ground Hawai'i biochar was also analyzed using a solid probe (4 mm) on the 300 MHz spectrometer, the spectrum was obtained from single ^{13}C pulse acquisition with high power decoupling and with a delay of 15 s between scans (number of scans 3200).

2.8.5 LC-MS

Un-ground biochar (BMC 07/09, 10 ± 0.1 g) was stirred with Milli Q water (MQ, 50 mL) for five hours. The mixture was allowed to settle overnight before centrifugation (10 min at 4000 rpm). The supernatant (~25 mL) was poured into a vessel, and freeze-dried overnight (Labconco Freeze dry systems) by using liquid nitrogen. The dry substance was then re-dissolved in MQ water (2 mL), and centrifuged before analysis.

2.8.6 GC-MS

This method was modified from reference 94
Sample (~1-2 g) was extracted in a Soxhlet apparatus with dichloromethane and methanol solution (DCM: MeOH, 95:5 v/ v, 200 mL) for 19-20 h. Longer times could not be used because the particulates (fine powder) of biochar sample would begin to penetrate the cell wall of a thimble and drain into extracts after 22 h. The solvents were removed under reduced pressure and the weight of the residue was recorded before being reconstituted in DCM: MeOH mixture (95:5 v/ v, 10 mL). The reconstituted solution (1 mL) was evaporated to dryness under a stream of nitrogen gas before being derivatized with Tri-Sil HTP reagent (1 mL, 20 min, 60 ˚C).

The derivatized sample was cooled to room temperature, and evaporated to dryness under a stream of $N_{2.}$ The residue was dissolved in heptane (500 μL). This reconstituted solution was mixed by a vortex mixer followed by centrifugation (2500 rpm, 5 min) before transferring the supernatant into a GC-MS vial with a flat bottom insert. Sonication of a sample was applied if white precipitate formed during the evaporation process.

Standard preparation

The following standards were prepared

Table 2.1 Summary table of standards used for GC/MS analysis

Standard	Purity	Solvent	Concentration (mg/ml)
D-Galactose	97%	MQ	0.961
D-Xylose	99.5%	MQ	0.941
Cholesterol	NA	MeOH	1.068
Glycerol	98%	MQ	1.003
D-Mannose	99%	MQ	1.171
Sucrose	99%	MQ	0.942
L-Arabinose	NA	MQ	1.174
D-Glucose	NA	MQ	1.289

Each standard (40 μL) was evaporated to dryness under a stream of nitrogen gas followed by derivatization with Tri-Sil HTP reagent.

Method Development

3.1 Laser Desorption-Ionization Time-Of-Flight Mass Spectrometry (LDI-TOF MS)

Sample preparation for LDI-TOF analysis is often quick and requires only a little effort; however in this study the efficiency of ion production of this technique has shown sensitivity to the sample preparation procedure. Although the sample preparation procedure was important, the preparation of the target was just as critical, therefore sample and target preparation methods were investigated and modified, along with instrument parameters to provide a quick, efficient procedure. Hawai'i biochar, 070706 (H.B) was used for method development due to the relatively abundant supply of this sample.

3.1.1 Sample preparation

This is the only step in the LDI process that is conducted outside the instrument. In the literature, sample preparation for LDI and matrix assisted LDI (MALDI) differs for soluble analytes (liquid) or insoluble material (solid). Insoluble solids have typically been mixed with solid matrix before target deposition whereas liquid samples are usually layered with matrix solution. Both of these methods were utilized and modified for any one sample in this study.

Initially the original sample* was suspended in the solvent system of choice, and mixed by a vortex prior to deposition on to the target plate with no addition of matrix.[69] Sample droplets were dried† before LDI analysis. It was found that sample particles did not adhere well to the target, making desorption difficult because laser ablation blows away sample particles. This was particularly so for biochar made from sucrose. Due to the complication with particle sizes and shape, this method was discontinued.

* Samples are generally received coarsely ground

† Ambient or warm air drying, dependent upon the volatility of the solvent used

To overcome the adherence issue, ground samples were trialled (sucrose biochar was used as an example). The sucrose biochar was ground with a mortar and pestle to very fine powder, suspended in a solvent and the procedure described above for target deposition was followed. A thin layer of charcoal powder was formed with sufficient adhesion to the target surface and the solvent was allowed to dry under ambient conditions. The large surface area reduced the contact angle of the ground charcoal particles with the target surface resulting in high surface energy, and more adhesion. Another advantage of this preparation was that extraction took place immediately between solvent and sample compared to un-ground sample (**Figure 3. 1**), thus the liquid* phase of a sample could also be analyzed. All samples were subsequently ground before analysis.

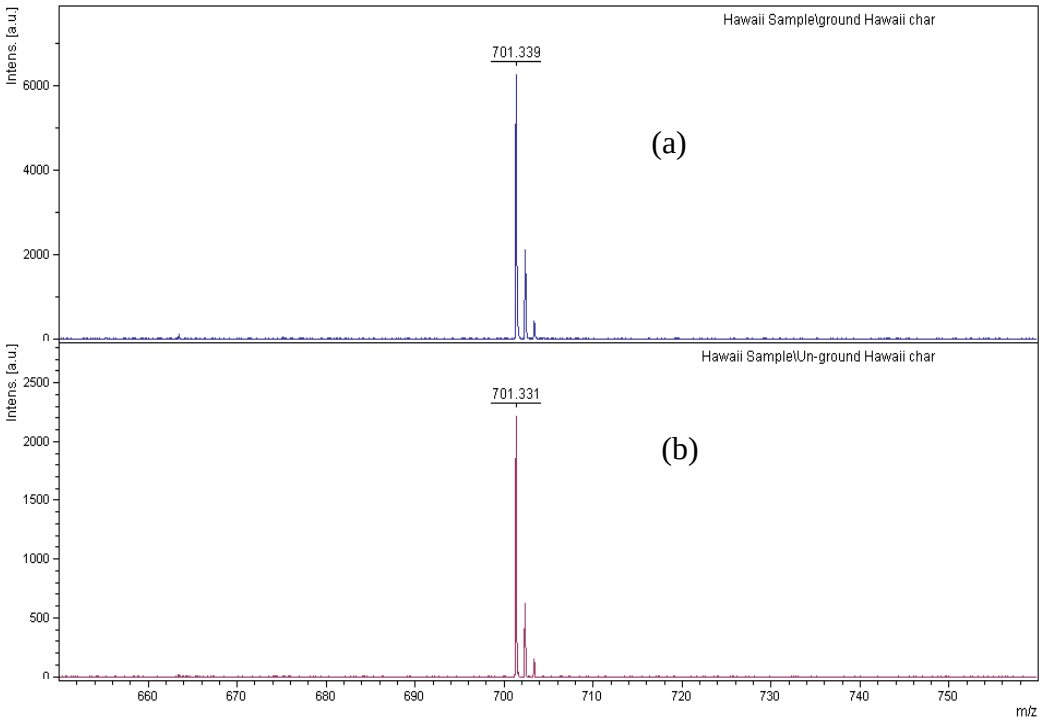

Figure 3. 1 LDI-TOF spectra of (a) ground and (b) un-ground sample

3.1.1.1 Choice of solvent for analyte extraction methods

For LDI analysis, samples were suspended in a solvent and the supernatant deposited onto the target cell. Solvents were considered suitable when a sufficient amount of the analyte of interest was extracted from the biochar sample resulting

* Supernatant of the solvent layer above biochar sample

in a reliable mass spectrum of the liquid. The solvent-based variability of analyte response made investigating a suitable solvent for this study necessary (**Figure 3.2**).

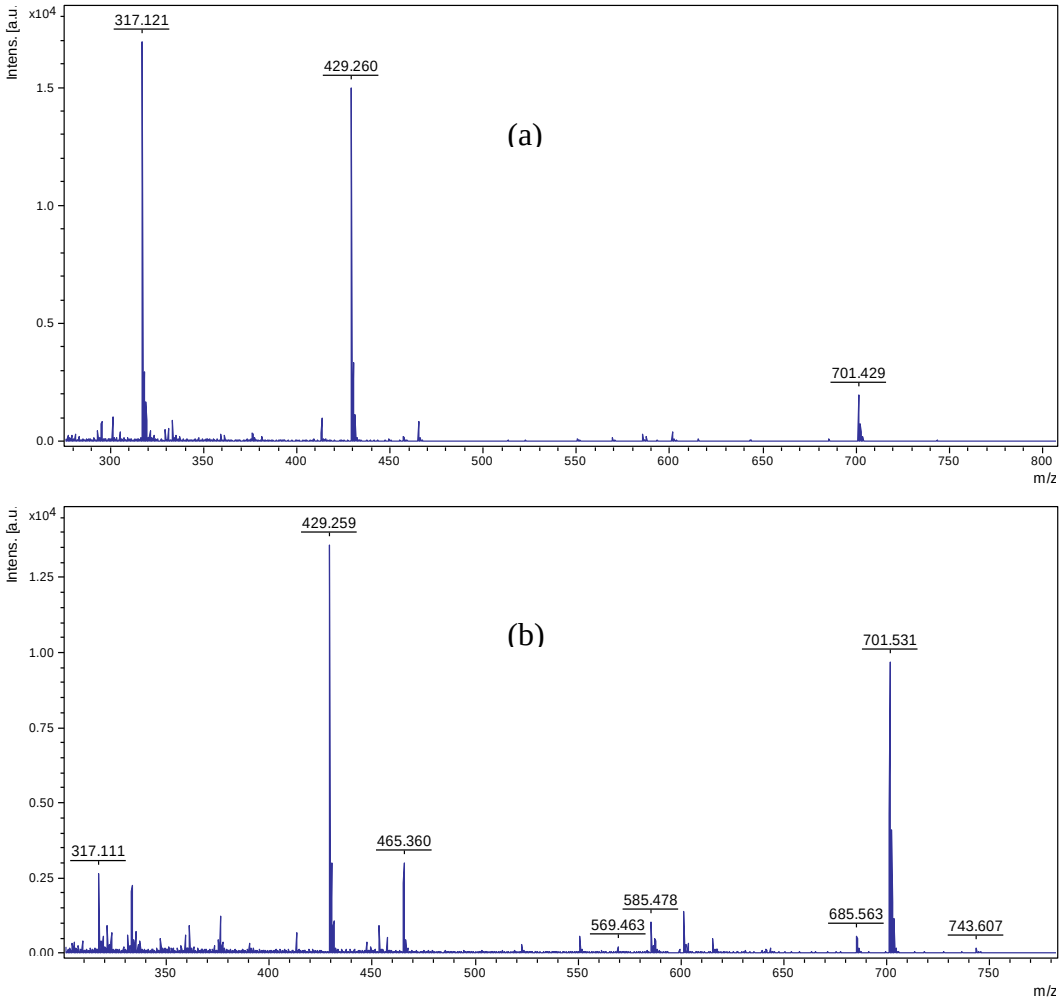

Figure 3. 2 LDI-TOF mass spectra of a ground BMC 06-09 biochar sample suspended in a solvent. (a) spectrum of the solid; (b) spectrum of the supernatant layer (solvent layer)

Rapid method

Acetonitrile and toluene have been reported as a suspension solvents[69, 67] for carbon cluster studies. They were both examined in comparison with acetone in reflectron mode. Acetone was chosen to be the suspension solvent due to its ability to partially extract the analyte of interest into the solvent layer to be analyzed separately to the solid, and also because of its high volatility, relative ease of spotting onto the target cell (either as aliquots or even with ground biochar

sample at the bottom of a micro-centrifuge vial) and because a clean spectrum[†]is obtained. Acetone is also miscible with methanol which was the dilution solvent that assisted ionization during MicrOTOF^{TM} analysis.

Extended method

This method was developed to suit different analyses. It was employed to increase the concentration of a characteristic biochar ion *m/z* 701 in the liquid phase. LDI-TOF MS enabled the rapid screening of the supernatant for the ion of interest prior to analysis with other instruments (NMR, MicrOTOF and GC-MS). A common laboratory solvent, methanol was trialled as a soaking solvent for biochar sample in comparison with acetone. After soaking the supernatant was transferred into a vial and clarified (Section 3.1.1.2), then spotted onto the target cell.

The supernatant from the MeOH resulted in a small peak of ion *m/z* 701which intensified with increasing laser power, with best intensity and signal-to-noise ratio at 50% and the carbon cluster region (200 *m/z* - 400 *m/z*) dominated the spectrum (**Figure 3. 3**). The maximum intensity of *m/z* 701 was < 200 a.u, indicating that the extraction or ionisation is not optimal with MeOH. On the other hand when acetone was used the *m/z* 701 peak is four times the intensity of that from MeOH and the carbon cluster region was relatively reduced. Therefore acetone was used as the suspension solvent in this method.

[†] Clean spectrum-a spectrum with less or no background noise

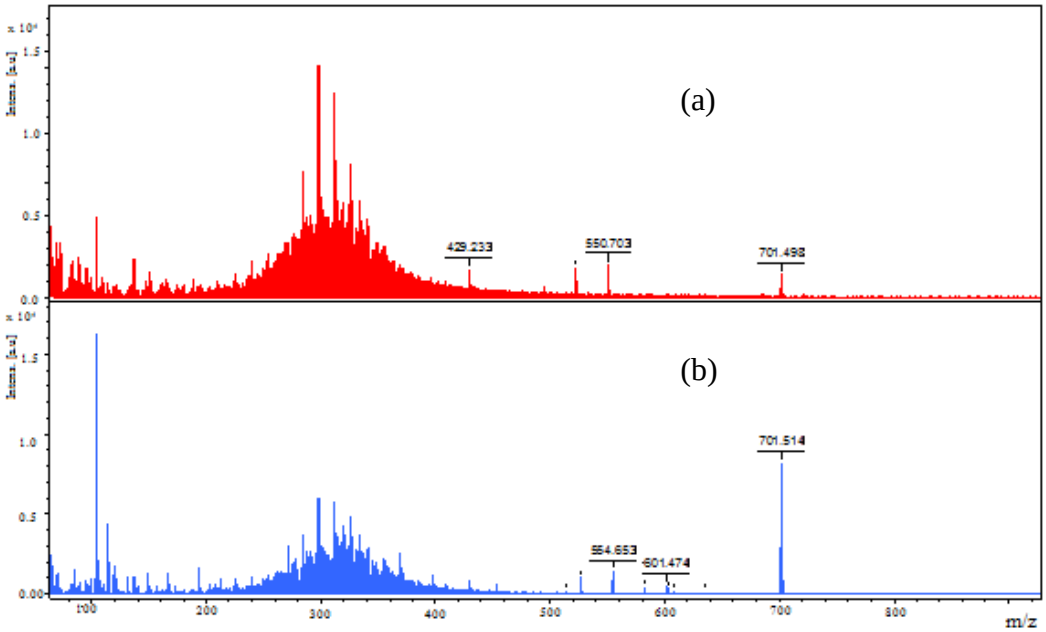

Figure 3. 3 LDI-TOF spectrum of supernatant of biochar sample soaked in (a) MeOH, (b) acetone

The results obtained by Bourke *et al.* (2007)[69] for linear positive mode analyses of biocarbon materials afforded a series of ions that were noted as characteristic peaks or fragments of biochar, such as *m/z* ions 317, 429,453, 465,685 and 701. Among those ions, *m/z* 317 did not always appear in extracts of biochar samples in this study. The ion *m/z* 429 was always present but in low intensity compared to the ions *m/z* 685 and 701 which were always present. A number of solvents were trialled to determine which were most efficient at extracting the *m/z* 429 ion into solution, in order to elucidate its molecular formula (**Table 3. 1**).

Table 3. 1 Solvents used and corresponding intensity of *m/z* 429 peak

	Solvent used	**Intensity (a.u.)**
1	Ethyl acetate (EtAc)	80
2	Isopropanol	38
3	ACN	39
4	DMSO + EtAc[a]	318
5	DMSO + EtOH[b]	43

[a] *100 µL DMSO stirred for 1 min followed by ethyl acetate (50 mL)*
[b] *100 µL DMSO stirred for 1min followed by ethanol (50 mL)*

Based on these results solvent system 4 was used to extract *m/z* 429.

3.1.1.2 Purification of *m/z* 701 after extraction

As for the extended method, finely ground biochar powders were soaked in an appropriate solvent for the chosen time (see Section 3.1.1.4). The mixture was allowed to settle before further clarification. Filtration with glass wool was trialled for removal of particulates of charcoal in the supernatant. However, the loss of compound of interest (*m/z* 701) due to the possibility of glass wool adsorption was unacceptable (**Figure 3. 4**). Therefore, an alternative filtration with a syringe filter (Cellulose acetate 0.45 μm membrane filter, Millipore) was examined; however the syringe filter was easily blocked with charcoal particles because of its pore size and the solution passed through gave approximately ten times less intensity of *m/z* 701 ion found in a centrifuged sample. The polarity of the molecule could mean that it becomes trapped in this filter membrane or on the particulates. Centrifuging the samples was found to be the most efficient method to clarify the liquid phase.

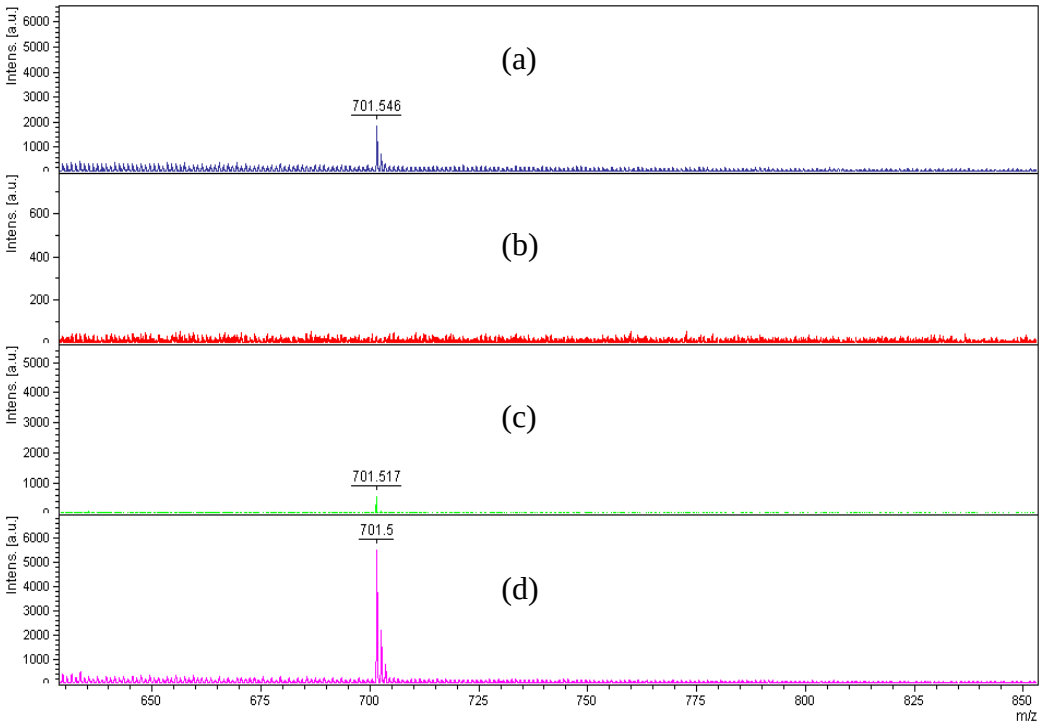

Figure 3. 4 Portion of LDI-TOF spectra for different sample purifications (a) un-treated acetone extract, (b) filtered with glass wool, (c) filtered with cellulose acetate syringe filter, (d) centrifuged

3.1.1.3 Choice of matrix

There is limited information on the analysis of organic extract (supernatant or liquid phase used in this study) of biochar associated with any matrix. Many studies have focused on analyzing or characterizing the charcoal in the solid phase. For example, 7, 7, 8, 8-Tetracyanoquinodimethane (TCNQ) was reported to show some success as a matrix for carbonaceous materials with high molecular weight (PHAs; MW up to 2708 Da, carbonaceous pitches; MW up to 1250 Da) [65, 66] using a solvent free sample preparation method. The solid phase of biochar without matrix gives a clean and high resolution spectrum. Therefore in this study, matrix solution (HCCA or DHB) was tested only for the liquid phase by either combination with the supernatant or direct application to the target cell separately in a layered manner.

The role of matrix is to absorb the UV laser light and transfer the energy to help ionize the embedded analyte molecules of the sample. The spectra obtained showed no significant difference between the supernatant alone and the sample with matrix application, thus the analyte of interest (*m/z* 701) is able to absorb laser energy light itself without the assistance of matrix. This indicates it is a highly unsaturated and/or aromatic compound. However, the matrix solution spotted on the target cell after sample deposition resulted in the absence of the analyte signal in the mass spectrum. This could be due to poor miscibility between the sample and matrix solution. Since the application of matrix had no obvious effect on increasing analyte detection, it was excluded throughout the research.

3.1.1.4 Effect of the soaking time on extraction of ion *m/z* 701

The length of time the biochar sample was soaked in a solvent affected the intensity of ion *m/z* 701 in solution samples. A series of soaking periods was investigated, 0.5 h, 2 h, 3 h, 5 h and overnight (17 h - 24 h).

The carbon cluster signals were intensified with increasing soaking time. The *m/z* 701 peak increased only up to five hours of soaking time. The result of overnight soaking showed that the ion *m/z* 701 was effectively diluted by extracted carbon

clusters as illustrated in **Figure 3. 5**. Thus, the soaking time of five hours provided the best abundance of ion *m/z* 701 and minimal carbon clusters.

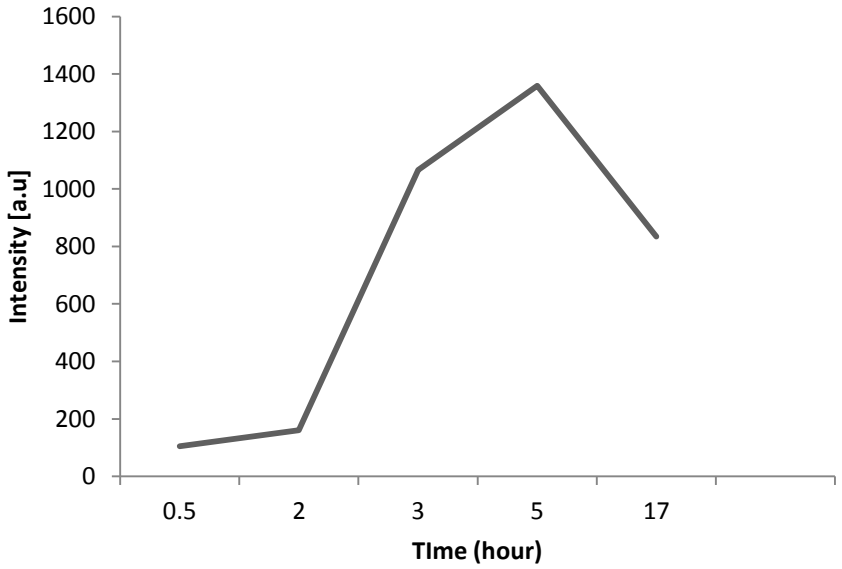

Figure 3. 5 Intensity of ion *m/z* 701 corresponding to soaking time

3.1.2 Target preparation

A stainless steel target was used for analyzing all the samples. Due to the possibility of residual contaminants left over from previous uses, it was necessary to develop a cleaning protocol to eliminate or reduce the unwanted signals produced from a contaminant material on the target.

The conventional cleaning protocol of a MALDI target is by applying aqueous methanol solution (50%, v/v) to the target then removing the impurities with a lint free tissue. Depending on the compound analyzed, wiping with MeOH solution might not be sufficient; hence a background check of the target cell was necessary before the sample analysis was commenced.

An example of a compound which is hard to remove from the target is fullerene. This compound was used as a target calibration standard for ion *m/z* 701, thus an alternative cleaning protocol was needed for removing this compound.
The cleaning protocol utilized in this investigation was sonication of the target in deionised water followed by sonication in 100% methanol (AR grade), and finally

again in deionised water (20 minutes in each solvent) and the target was then dried using lint free tissue. This cleaning protocol effectively removed fullerene and reduced contaminants residing in grooves but despite this occasionally traces were found to reside on the target.

3.1.3 LDI-TOF MS parameters

3.1.3.1 Laser power

It is crucial to have the optimum laser power as, if it is too low, the loss of signal to noise ratio could mean poor resolution or that no analyte ions will be observed, whereas too high laser power leads to a high background level and an oversaturated spectrum.

A series of experiments utilising different laser powers of 40%, 45%, 50%, 60%, were applied to a control sample (Hawai'i biochar suspended in acetone). The spectrum below (**Figure 3. 6**) shows the relative intensities obtained using the different laser powers.

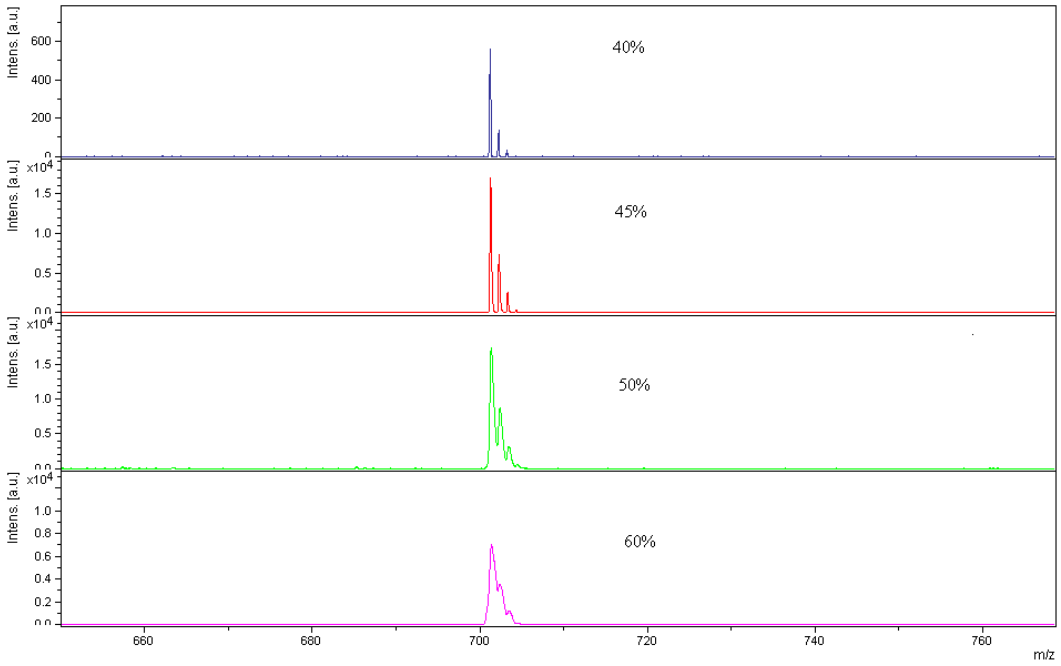

Figure 3. 6 Spectra of Hawai'i biochar analyzed at different laser power

These spectra show the difference in signal intensities obtained at different laser powers is substantial. The spectrum at 40% laser power showed poor signal

intensities, and the increased background intensities of those at 50% and 60% laser power were detrimental for analysis of the ions of interest, leading to the choice of laser power for this study being 45%.

3.1.3.2 Number of Laser shots

Bourke *et al.* (2007)[69] summed 300 shots consisting of 30 shot samples repeated ten times within a single spot on the target. In this study, samples were analyzed in triplicate (3 spots) to ensure the reproducibility. Each of the spots was summed 210 shots consisting of 30 shot samples repeated seven times as a typical mass spectrum with good signal-to-noise ratio requires about 50-200 shots.[70] The intensity for any individual ion measured is proportional to the concentration of the analyte which gives rise to that ion and it is only comparable between spectra if the number of shots is kept the same for each sample throughout the study. It is not possible to make judgements about relative concentrations within a single spectrum because concentration is only one factor affecting ion intensity.

3.1.3.3 Determination of mass ranges

The determination of mass ranges is also an important part of analysis due to the fact that an excessive mass range makes it difficult to interpret peaks of interest but a mass range that is too small could result in the exclusion of an ion related to the ion of interest. Therefore the initial mass range involved was up to 2000 *m/z* to avoid missing any possible parent molecular ions of *m/z* 701 or a dimer ion of *m/z* 701. However, there was no indication of a dimer ion $[2M+H]^+$ (1401 *m/z*) and no other peak beyond 1000 *m/z* was observed. Thus the mass range used in the study was up to 1000 *m/z*. In addition, in order to prevent detector saturation, ions less than or equal to 40 Da were suppressed.

3.1.3.4 Instrument configurations

The Bruker Daltonics Autoflex II MALDI-TOF is equipped with configurations such as linear mode for screening applications, reflectron mode for identification and TOF/TOF technology (LIFT^{TM}) for characterization. All spectra were acquired in positive ionization in which *m/z* 701 was initially observed by Bourke *et al.* (2007)[69]

Linear mode and reflectron mode

The choice of the best operating mode depends on the signal intensity and resolution required. The resolving power of a TOF analyzer is mass dependent and also a function of the length of the flight path.[71] Therefore, it is important to ensure that a suitable mode is used for analyses.

The reflectron and linear modes were both operated on a control sample that was prepared as described in Section 2.1.2. Spectra obtained from both operation modes of mass spectrometer showed no significant difference in the mass range up to 300 *m/z*; however a lack sensitivity of ion *m/z* 701 was observed in linear mode (**Figure 3. 7**). Ions that are detected in linear mode are the parent ions or ions that resulted from decomposition of parent ions during flight. These decomposed ions would have same kinetic energy as the parent ion they arrive at the detector at the same flight time as the parent ion thus resulting in a broad peak. In reflectron mode, ions are reflected back based upon their current mass and therefore the decomposed ions no longer contribute to the signal for the parent ion which leads to the loss of a signal. Any ion whose signal is the same or more intense in reflectron mode compared to linear mode is stable to post-source decay (PSD).[71- 73] This indicates that the *m/z* 701 is the signal of a stable ion. Thus it was decided that reflectron mode should be used for this study.

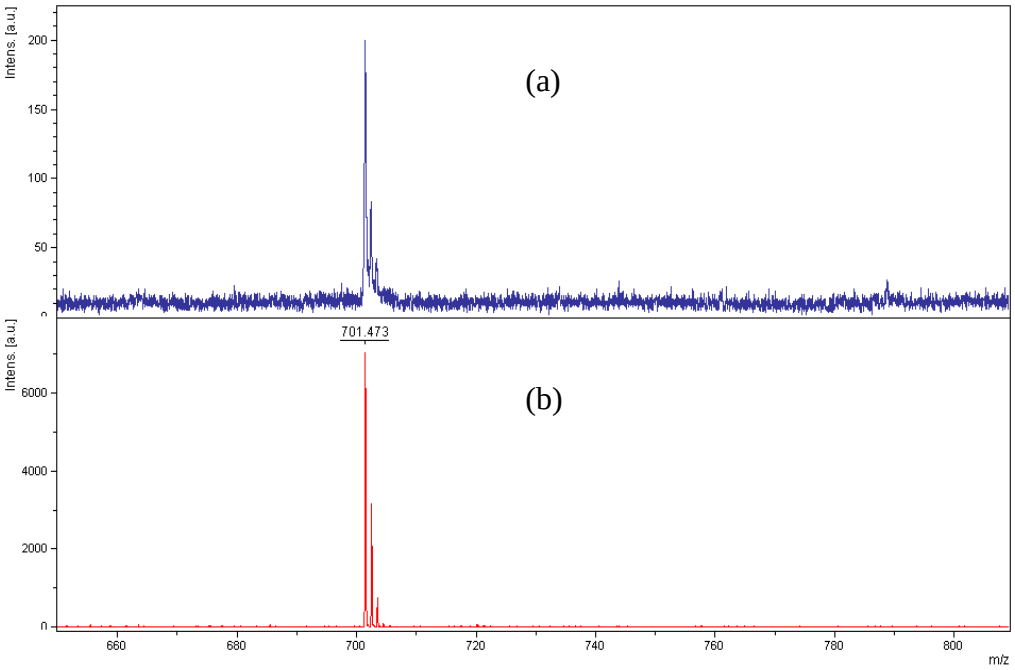

Figure 3. 7 LDI-TOF spectra of Hawai'i biochar obtained from (a) linear mode and (b) reflectron mode at 45% laser power.

LDI-TOF/TOF (LIFT^{TM})

LDI-TOF/TOF is a technique used to characterize the ion (s) by causing them to fragment and examining daughter ions. However, no fragmentation of *m/z* 701 occurred which again indicates the stability of this compound. It also agreed to the result obtained by Bourke *et al.*[69] Consequently, another method needs to be investigated for further understanding the compound's structure.

3.1.4 Soxhlet extracts analyzed by LDI-TOF

The organic extracts (DCM:MeOH, 95:5 v/v) from the Soxhlet extraction of a control sample before and after evaporation and reconstitution were analyzed by LDI for ion *m/z* 701.

Soxhlet extraction solution before evaporation (solution A)

To provide sufficient sample for analysis, several layers of solution A were spotted on a target cell that was previously checked for background and this was air dried before analysis due to the relatively high volatility of extraction solution. This was carried out without matrix (see **Figure 3. 8**).

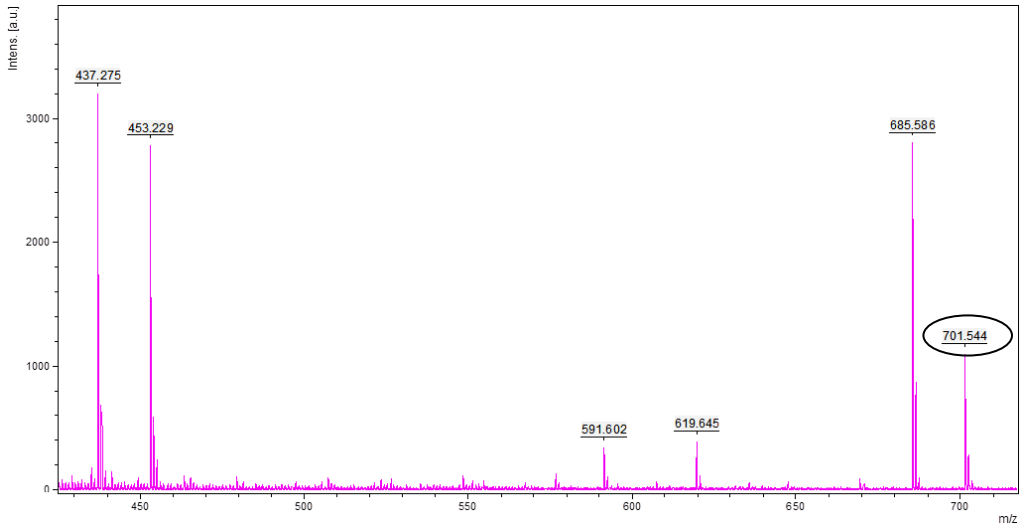

Figure 3. 8 Portion of LDI-TOF spectrum of DCM:MeOH, 95:5 extract of Hawai'i biochar (reflectron mode; 45% laser power)

Soxhlet extraction solution after evaporation (solution B)

A similar analysis of the extract that had been evaporated and reconstituted (Section 2.2.3) is shown in (**Figure 3. 9**).

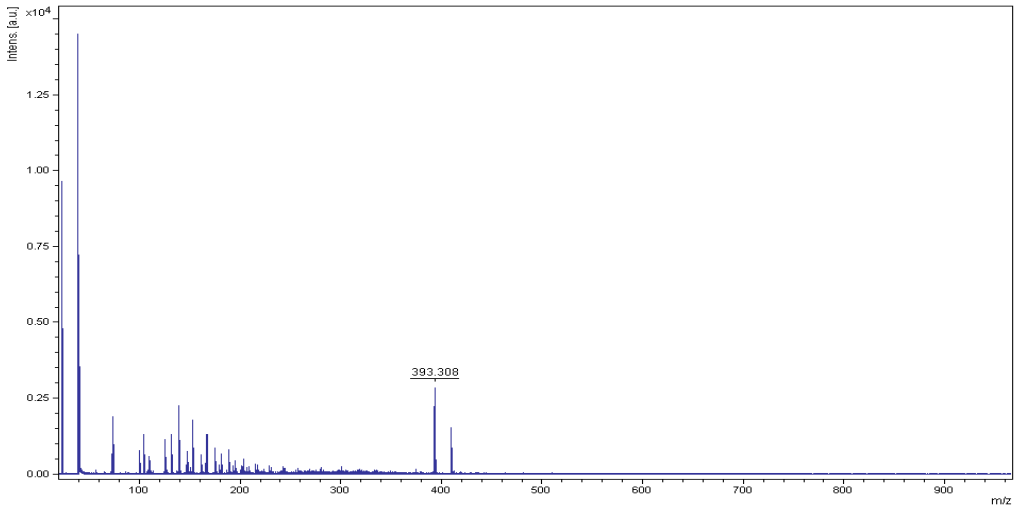

Figure 3. 9 LDI-TOF spectrum of DCM/MeOH extract of Hawai'i biochar after evaporation and reconstitution (reflectron mode; laser power 45%)

There are distinct differences between solution B and solution A. Solution A contains detectable amounts of ion *m/z* 701 and other discrete ions which are the characteristic biochar ions. The spectrum of solution B showed no sign of the 701 *m/z* peak even with matrix used but contained ions with *m/z* value 393 and 409.

It is possibly that the ion *m/z* 701 was strongly bonded to solvent molecules which have undergone evaporation, condensation and collection in the solvent waste reservoir of a rotary evaporator. Although, it is unlikely that a molecule which contains mainly carbon can be easily evaporated, for example fullerene and graphite. However, after the solvent evaporation of solution A, oily residues were formed (the colour and amount depends upon the biochar sample extracted) in the flask. Possibly the molecule dissolved in the DCM solution previously was separated from the solution in a solid form during evaporation and changed its chemical/ physical properties and would not redissolve.

3.2 Gas chromatography mass spectrometry (GC-MS)

To permit analysis of compounds that have inadequate volatility or stability by GC-MS, derivatization is required. The two commonly used silylation reagents TMSI and Tri-Sil HTP were trialled in comparison on a control sample extract.

A known amount (5-10 mg) of control sample was derivatized by 400 μL pyridine with 400 μL TMSI or 1 mL Tri-Sil HTP (60 ˚C, 20 min). Sample were evaporated to dryness under a stream of N_2 gas and reconstituted in heptane. With TMSI, re-crystallization over a short period of time was observed in heptane. These crystals can cause blockage in the injector depending on the number of solvent washes before and after injection. In addition, the chromatogram of the solution derivatized with TMSI resulted in an unresolved region occurring around 10 min, as shown in **Figure 3. 10**. Neither of these effects was observed in sample solution derivatized by Tri-Sil HTP reagent and the chromatogram obtained gave well separated, resolved peaks. Therefore, Tri-Sil HTP was chosen to be the silylation reagent for further sample analyses.

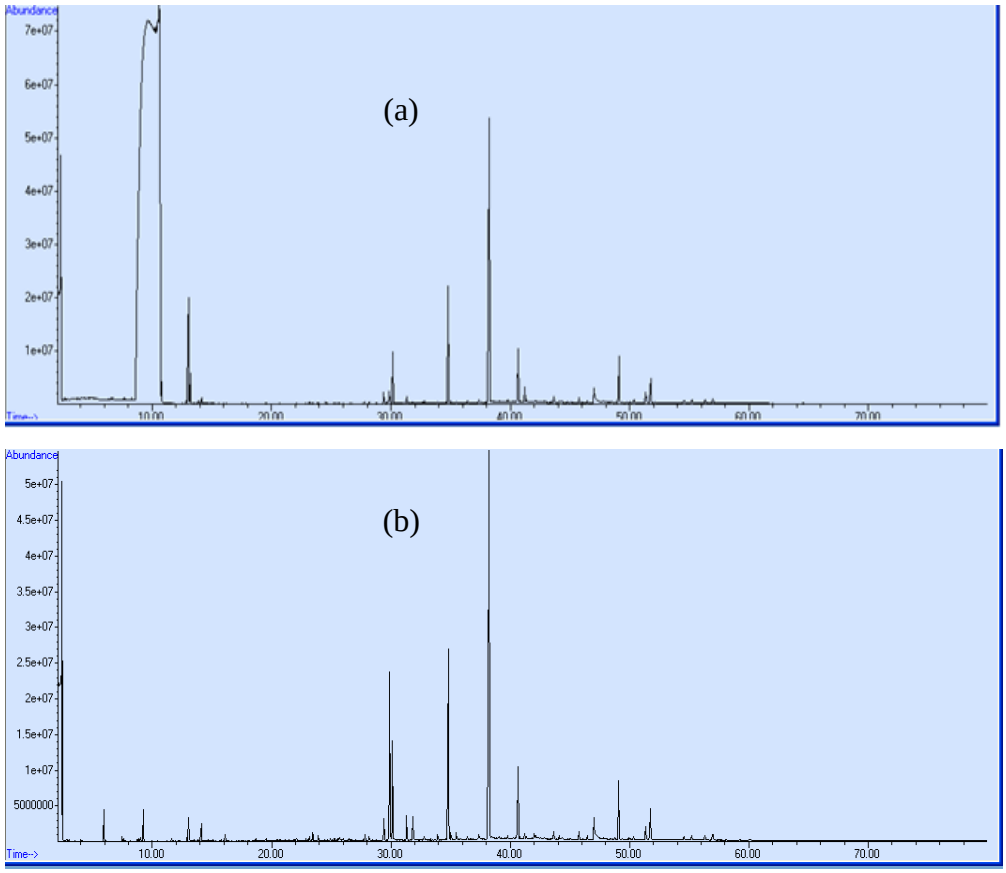

Figure 3. 10 GC-MS chromatogram of organic extracts: (a) organic extract derivatized using TMSI reagent (b) derivatized using Tri-Sil HTP reagent

Investigation of characteristic ions of biochar

The formation of biochar is a complex process, of which the mechanism of the steps is not well understood yet. However, a discrete ion series were proposed by Bourke *et al.*[69] as characteristic of biochar. A large amount of information has been obtained by researchers studying the plethora of reactions involved in the pyrolysis process, yet there is still a lack of information on an accurate model of the chemical structure of biochar. In this study, instrumental techniques including LDI-TOF- MS, ESI-TOF-MS, NMR and LC-MS have been employed and the information obtained will be discussed in the following sections.

4.1 Molecular mass determination of characteristic biochar ions

In agreement with the LDI result obtained by Bourke *et al.*,[69] in this study positive reflectron mode analyses of biochar afforded a series of discrete ion pairs with mass values separated by 16 amu (**Table 4. 1**), this was attributed by Bourke *et al.*[69] to the difference of an oxygen atom. In this study inconsistency of peak ratio between each pair, for example *m/z* 685 and 701, was observed among biochar samples. Alkali metal ions are commonly present in biochar and the mass spectrometer can show adduct ions, such as $[M+Na]^+$ or $[M+K]^+$, which have a mass difference of 16. A sample extract with sodium chloride (NaCl) or potassium chloride (KCl) solution added as a cation source was trialled. Analyses of sample extract with or without salt addition were carried out on the same day for comparison.

Table 4. 1 Table of ion pairs observed and their corresponding molecular mass

Characteristic ions (*m/z*)	Ion pair with 16 amu difference (m/z)	Actual molecular mass
317	301	278
429	413	390
453	437	414
465	449	426
701	685	662

Positive reflectron mode analyses of biochar extract spiked with NaCl and KCl showed that the intensity of peak 685 *m/z* was increased with corresponding reduction of the *m/z* 701 peak when additional Na^+ ion was added (**Figure 4. 1b**). The contrary effect occurred with the addition of K^+ ion (**Figure 4. 1a**), addition of rubidium ion caused the appearance of an ion *m/z* 747 corresponding to $[K+Rb]^+$ (**Figure 4.1c**). Thus each pair of ions represents preseudomolecular ions of a single compound, with respect to sodium $[M+Na]^+$ and potassium $[M+K]^+$ (a difference of 16). Thus the actual molecular mass for the pair *m/z* 685/701should be 662. The other characteristic peaks also behaved in the same way so the molecular mass of those ion pairs should be 278, 390, 414 and 426 respectively as shown in **Table 4. 1**.

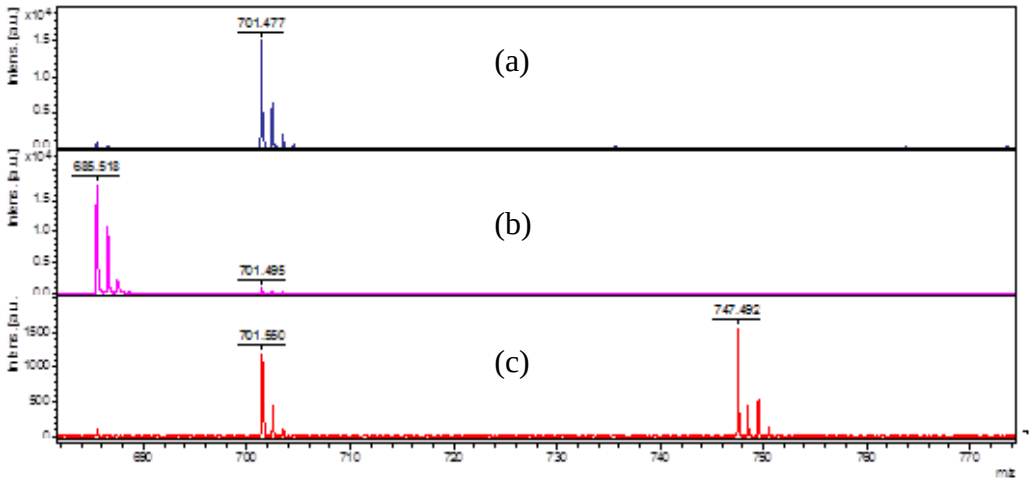

Figure 4. 1 Spectra of biochar extract spiked with different alkali metal ion (a) potassium adduct (b) sodium adduct (c) rubidium adduct

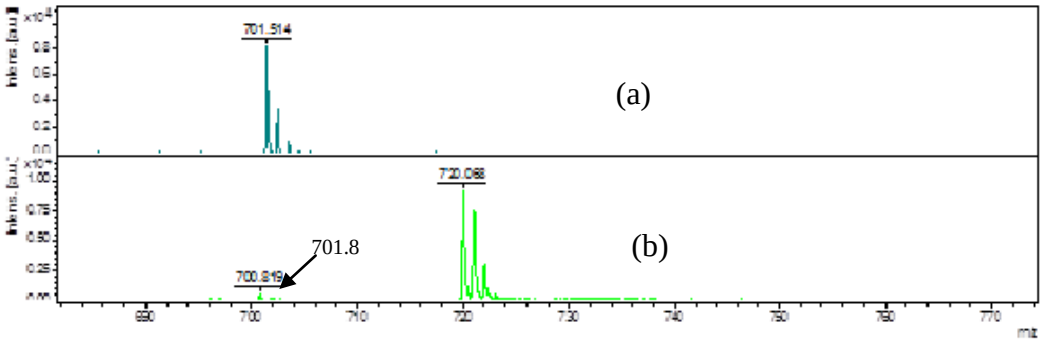

Figure 4. 2 Spectra of biochar in comparison with fullerene (a) Hawai'i biochar (b) fullerene standard (C_{60})

Spectra resulting from the analysis of biochar or its extract differed from those obtained from the fullerene C_{60} standard since no *m/z* 720 was observed. However, fullerene also afforded an ion *m/z* 701 (**Figure 4. 2b**). The mass value observed in the mass spectrometer is usually within 1 Da of the expected mass.[72] The expected mass depends on the peak observed, which is unclear the for ion *m/z* 701 shown in **Figure 4. 2b**, it could be an isotopic peak of 700.8 *m/z* or an unresolved peak. If it is unresolved the peak mass observed would be the average mass,[74] if it is a resolved peak the expected mass would be the mono-isotopic mass or mass of an isotope peak.[72] To discover whether *m/z* 701 observed in biochar is a fraction also found in fullerene, a comparison was carried out. The spectra (**Figure 4. 3a**) illustrates the peak of *m/z* 701 is not the same in biochar as in fullerene. Sample extract spiked with fullerene standard was also analyzed as confirmation. As illustrated in **Figure 4. 3 b**, the mixture of biochar extract with fullerene obtained two peaks with *m/z* value of ~ 701. The peak *m/z* 701.5 which is not overlaid with any other peaks, was obtained from fullerene only (red), this reveals that the compound of interest in biochar is not a same fraction also found in fullerene.

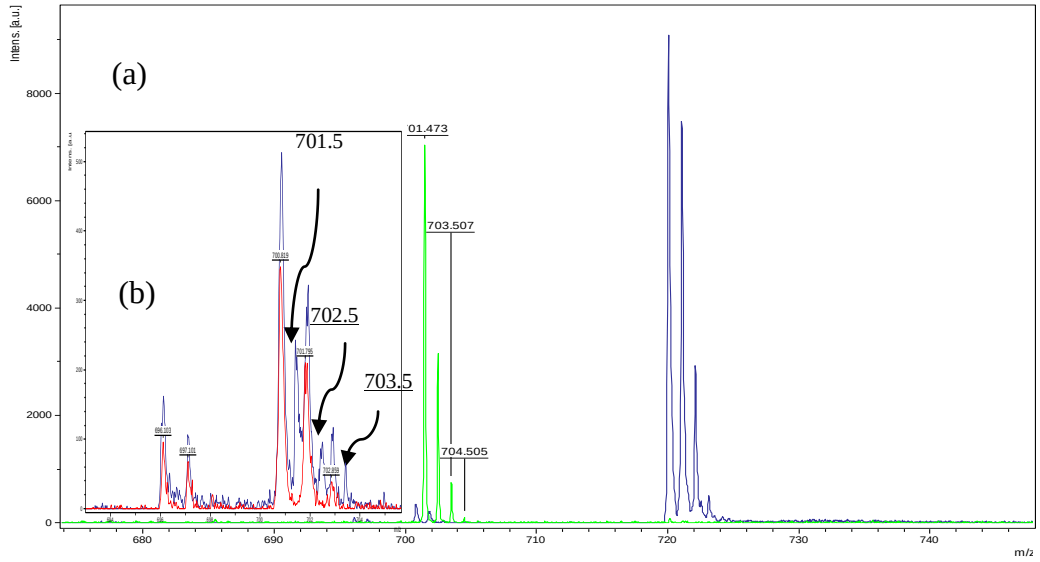

Figure 4. 3 An overlaid spectrum of fullerene (C_{60}) standard with a control sample; (a) spectrum of biochar in green overlaid with a spectrum of fullerene (b) expanded spectrum of 701m/z region; mixed fullerene with control sample in blue, fullerene in red.

Bourke *et al.*[69] have proposed some structures for characteristic ions observed in LDI. From the adduct ions tests, the results show the molecule that gives rise to the ion *m/z* 701 has molecular mass of 662 and it is not same fraction also found in fullerene. From here on this molecule is referred to as **molecule X**. A model structure should be based on this mass rather than 701.

4.2 Structural elucidation of the compound which gives m/z 701 (Molecule X) with other techniques

4.2.1 NMR

NMR is a powerful technique for structural elucidation. A 400 MHz NMR was used to analyze sample extract obtained from the extended method (Section 2.8.1) with further modification by dissolving in deuterated MeOH. Several NMR experiments were carried out including HSQC, HMBC, DEPT, ^{13}C and ^{1}H. Due to the large amount of signals in the carbon and proton spectra arising from a variety of carbons possibly from different compounds it was not possible to use these results to elucidate the structure of molecule X. NMR is very much less sensitive than mass spectrometry, so a higher concentration of molecule X would be required. Since there is a wide range of possibilities of carbon based structures

within the sample including carbon clusters, it is extremely difficult to distinguish which peaks are associated with the compound of interest. An experiment on biochar using a solid probe (4 mm) was performed at 300 MHz. The spectrum which resulted from the solid state NMR did not provide any additional information on biochar structure. As expected the main peak was in the aromatic region **(Figure 4.4)**; the peak at 27.4 ppm indicates aliphatic carbon, but may be adsorbed material such as plasticizer; the aromatic region is between 100-150 ppm. Two broad peaks on each side of the aromatic region at ~189 and ~55 ppm are the spinning side bands.

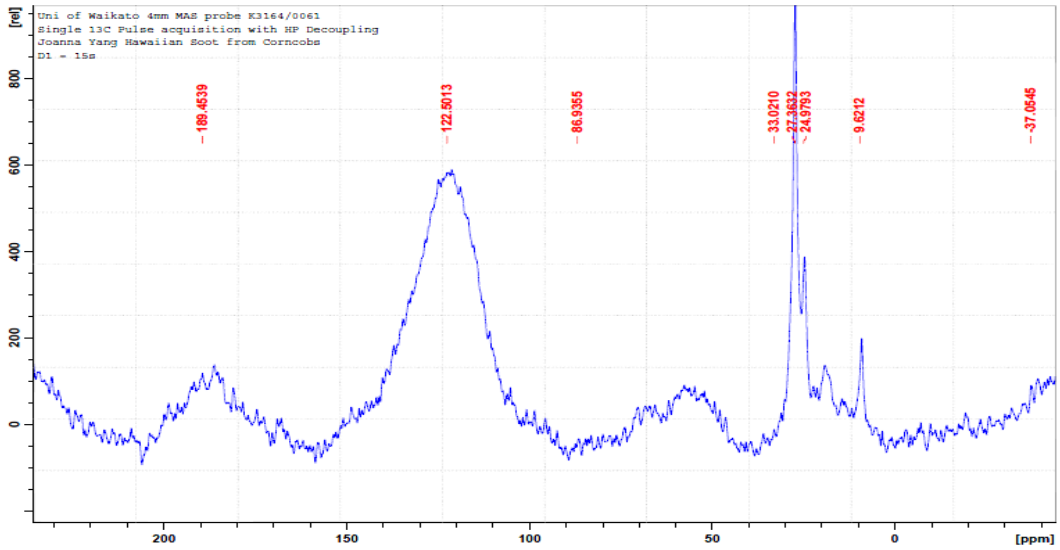

Figure 4. 4 Solid state NMR spectrum of Hawai'i biochar

4.2.2 GC-MS

GC-MS analysis was also employed for studying the structure of molecule X. Sample was soaked in acetone (refer to section 2.1.5), the supernatant was transferred into a GC vial and directly injected into the system.

The full scan mode and selected ion mode (SIM) were the two basic operational modes in GC-MS. Scan mode is useful in identifying unknown compounds in sample. It provides more information in confirming or resolving compounds in sample. SIM provides higher sensitivity (low detection limits) as the instrument can be set up for only monitoring specific ion and its fragments. Therefore, both modes were utilized to determine the ion *m/z* 662 and its possible fragments, on sample extract obtained as above.

The spectra showed no presence of ion *m/z* 701 as expected. However, using an extracted ion chromatogram technique, a peak of *m/z* 662 was obtained, **Figure 4. 5**. GC-MS is an analytical technique that measures mass-to-charge ratio of charged particles, and can be utilized for elucidating the chemical structures of molecules but one of its disadvantages is the mass detection range. The total mass range extends to 800 amu; if the source is in any way contaminated loss of sensitivity at high mass can occur. The molecule X, *m/z* 662 is on the high border side of mass range, the sensitivity of detection would be relatively low.

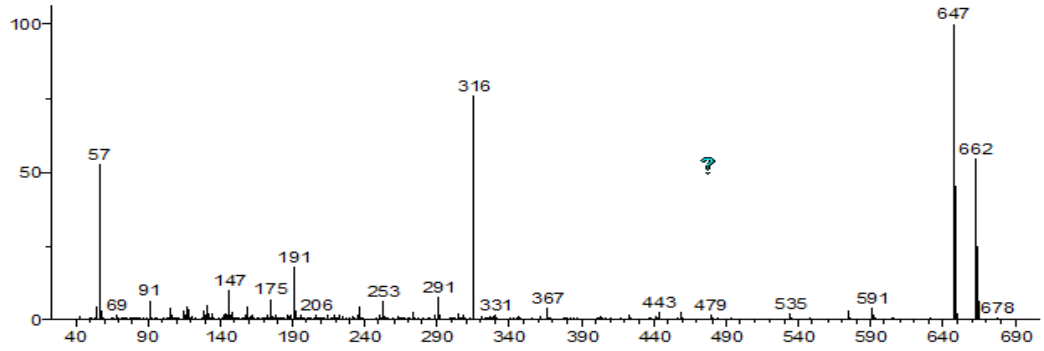

Figure 4. 5 EI mass spectrum of a compound of interest

The peak at *m/z* 662 could possibly be the molecular ion of the compound X. The intensity of this molecular ion and fewer fragments indicate an aromatic compound. The fairly late retention time (at 56 minutes, 300 ˚C) on the column, suggesting that it has high aromaticity and lack of volatility. Both of these features agree with the studies carried out previously. The difference between the predominant peak at *m/z* 647 and 662 is from the loss of a methyl group, suggesting that the molecule X could contain a methyl group (**Scheme 4.1**). The prominent peak at 316 is suggestive of some sort of tropylium ion or very stable fragment. In order to obtain these fragments, the structure of molecule X could possibly contain two aromatic systems linked by a CH_2 group. The group on one side of this CH_2 group could contains a methyl ketone group that linked to an aromatic ring which can easily cleave off to give the fragment *m/z* 647 as an acylium ion, and cleavage next to CH_2 would give the formation of tropylium ion (**Scheme 4.2**).

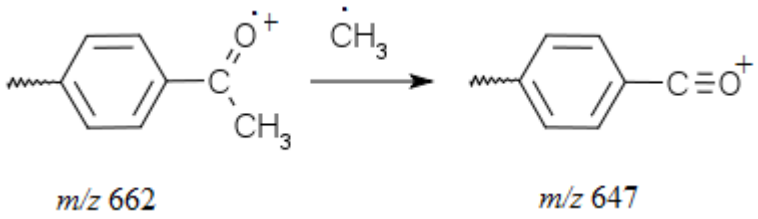

Scheme 4.1 A possible formation of an acylium ion

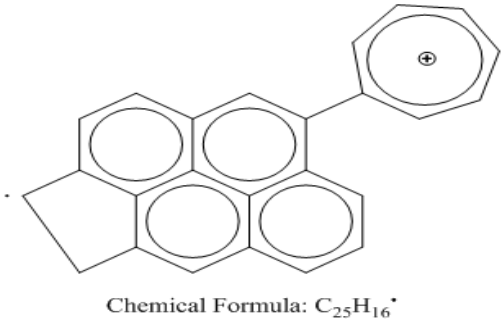

Scheme 4.2 A possible tropylium ion of *m/z* 316

4.2.3 LC-MS

From the LDI-TOF study, a molecular mass was determined. To elucidate the structure of mass 662, ion trap LC-MS was employed.

Biochar sample was extracted with MQ water and was concentrated using the freeze dryer. The dry substance obtained was re-dissolved in water (2 mL). This reconstituted solution was analyzed by LDI-TOF for ion *m/z* 701 before proceeding to analysis with LC-MS. It was necessary to perform a preliminary test for the compound of interest because a different extraction solvent and protocol was employed.

APCI was chosen as the ion source because it is capable of detecting relatively non-polar compounds which is what the compound of interest was believed to be. Similar to ESI, the sample extract was introduced into the ionization source directly; however with the APCI source sample droplets were rapidly desolvated/vaporized by its heated vaporizer rather than by electrostatic charge.

With direct infusion an ion with *m/z* value of 663, $[M+H]^+$ was observed. Proton transfer occurred because the chemical ionization of analyte molecules is efficient, and the collision between analyte and reagent ions is rapid at atmospheric pressure. The typical adduct ions seen in LDI-TOF were not observed. However a series of fragments were obtained from the application of MS/MS^n with a mass difference of 56 amu such as *m/z* 607, 531 and 495 (**Figure 4. 6**). Sample extract was also introduced via HPLC using a C_{18} column; the elution time of the compound was at 9.6 min with 80% MeOH as mobile phase, **Figure 4. 5**. Multiple runs were performed for confirmation. The ease of fragmentation is unlike the observations in LDI-TOF mass spectrometer and given the aqueous solvent it is likely that this is not the same ion. The repeating unit of 56 suggests some sort of polymeric structure. Therefore these results must be viewed with caution.

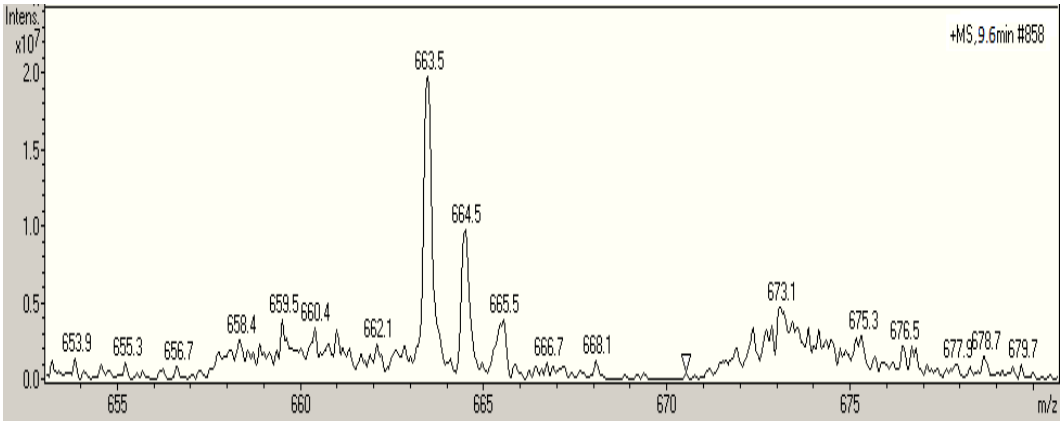

Figure 4. 6 LC-MS chromatogram of compound X eluted at 9.6 minutes

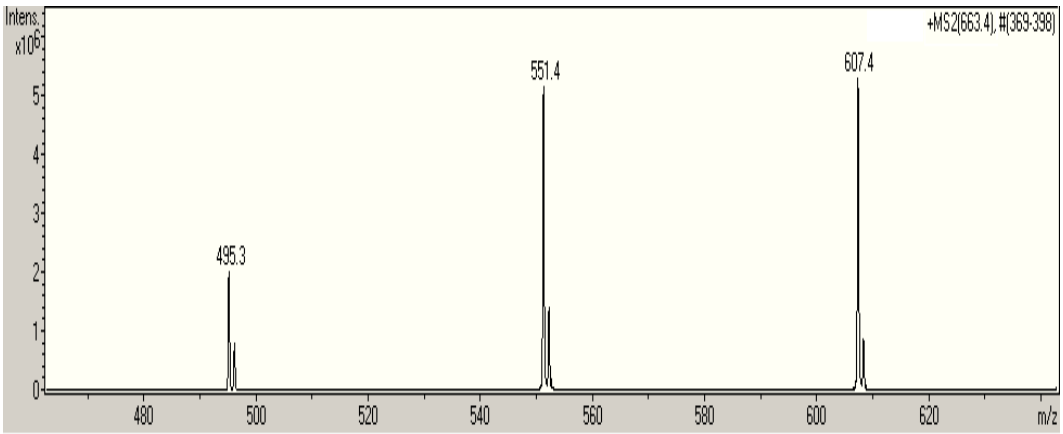

Figure 4. 7 MS/MS^n fragmentation chromatogram of *m/z* 663

4.2.4 ESI-TOF

The organic biochar extracts were diluted with MeOH to give a concentration of ~0.1 mg/mL solution. The diluted solution was introduced into the mass spectrometer *via* a syringe pump. As shown in the **Figure 4. 7**, the two prominent peaks are the desired sodium and potassium adducts of molecule X. The Smart Formula tool was utilized to predict the molecular formula of these two adduct ions.

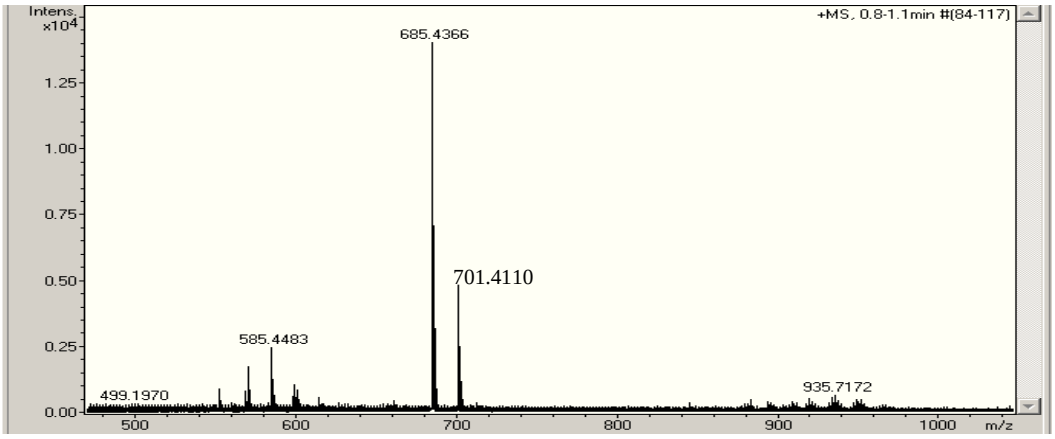

Figure 4. 8 ESI-TOF mass spectrum of biochar organic extract

Table 4. 2 Molecular formula for molecule X

Mass	Formula	Score	m/z	err (ppm)
685.4366	$C_{49}H_{58}NaO$	100	685.438	1.4
701.4110	$C_{49}H_{58}KO$	100	701.4119	0.9

The formula for both peaks at *m/z* 685 and 701 was generated with a tolerance value of 20 ppm. This tolerance value if it is too small the possible formulae obtained would be limited; if it is too big a wide range of formula would be generated with lack of mass accuracy. The two formulae obtained in **Table 4. 2** show a mass accuracy of much better than 3 ppm which is the general criteria for a formula determination with internal calibration. The formulae differ only by the Na and K adducts which once again indicated that both the characteristic peaks of biochar are from the same compound. The molecular formula determined by ESI-TOF in combination with the mass unit difference observed from LC-MS analyses which contribute additional information that allowed modelling of a possible structure for this molecule X (See Appendix 1).

4.3 Identification of plasticizers in biochar samples

4.3.1 Introduction

Plasticizer is added to plastics to improve their flexibility and workability, the most widely used plasticizers are phthalates which are derived from phthalic acid.[75] Globally, millions of tons of phthalate are produced annually.[76] Phthalates are primarily used as softener in polyvinyl chloride (PVC) and in a wide variety of products such as supermarket bags and food containers, medical tubing and blood bags, chemical containers and electrical devices. Because they are not chemically bound to plastic, they can be leached out, migrated or evaporated thereby becoming environmental contaminants.[77] Traces of these compounds often interfere in analytical techniques.[78]

The common plasticizers are listed in **Table 4. 3**.

Table 4. 3 Common plasticizers and their adduct ions[79]

Plasticizer	Mass to charge ratio (*m/z*)		
	M	**M+Na**	**M+K**
dibutyl phthalate (DBP)	278	301	317
benzyl butyl phthalate (BBP)	312	335	351
Hexanedioic acid	370	393	409
dioctyl phthalate (DOP)	390	413	429
diisononyl phthalate (DINP)	418	441	457
diisodecyl phthalate (DIDP)	447	470	486

Any technique has the potential to introduce contaminants into the system; therefore modern analytical methods that follow good laboratory practice use blank tests and ultrapure chemicals and reagents to minimize any background interference.[78] In this study, several blank tests have been performed to identify the possible contaminants and their origin.

4.3.2 Solvent and pipette testing

Solvents that were involved in the extraction of ion *m/z* 701 were investigated. DCM, MeOH and acetone used in this study were tested individually with 2 types of pipette that are commonly used in the laboratory. All the solvents used were taken from newly opened bottles and the analyses were carried out on the same day to eliminate any preventable cross contaminations.

The MALDI target was thoroughly cleaned and tested before the solvent was deposited. Solvent was spotted exactly on the target cell that has been previously checked for background using either an autopipette or a pasteur pipette. The results showed ions with *m/z* values of 413, 429 and 449. There were significant amounts of these ion after background subtraction whichever pipette was used (**Figure 4. 9**, **Figure 4. 10** and **Figure 4. 11**), but there was more from the pasteur pipette suggesting that these ions are potential interference peaks. There is the possibility that these ions represent phthalates which may come from various sources (**Table 4. 3**).

This was confirmed by high resolution mass spectrometry (ESI-TOF). A sample that was extracted using the extended method (refer to Section 2.8.1) was analyzed for identification of those interference peaks. The results are listed in **Table 4. 4** show that *m/z* values 317, 429, 453 present in the biochar extract could possibly be plasticizers rather than a structural building block for biochar.

In LDI the intensity of these ions were more with the glass pasteur pipette than with autopipette. The plasticizer contaminant sources could be pipette tips, bottle caps, and plastic containers or filter membranes. The results for the glass pasteur pipette suggest contamination by exposure to the general environment[80] should be taken into consideration. Biochar is particularly good at adsorbing organic

compounds so is likely to be rapidly contaminated with plasticizers from the general environment.[1]

In the literature, three quaternary ammonium compounds have been identified[78] as strong background peaks in LDI mass spectra. These include dimethyl-dihexadecy-ammonium, dimethyl-hexadecyl-octadecyl-ammonium and dimethyl-dioctadecyl-ammonium with *m/z* values 494, 552 and 550 respectively. These were observed as background, **Figure 4. 9** and could possibly come from personal care products as they are usually used in cosmetics.[81]

Table 4. 4 Identified contaminate compounds by MicrOTOF

Mass m/z	$[M+X]^+$	Formula	Compound Name
301	$[M+Na]^+$	$C_{16}H_{22}O_4$	Dibutylphthalate
317	$[M+K]^+$		
413	$[M+Na]^+$	$C_{24}H_{38}O_4$	Diisooctylphthalate
429	$[M+K]^+$		
437	$[M+Na]^+$	$C_{18}H_{38}O_{10}$	Nonaethylene glycol(PEG-9)
453	$[M+K]^+$		

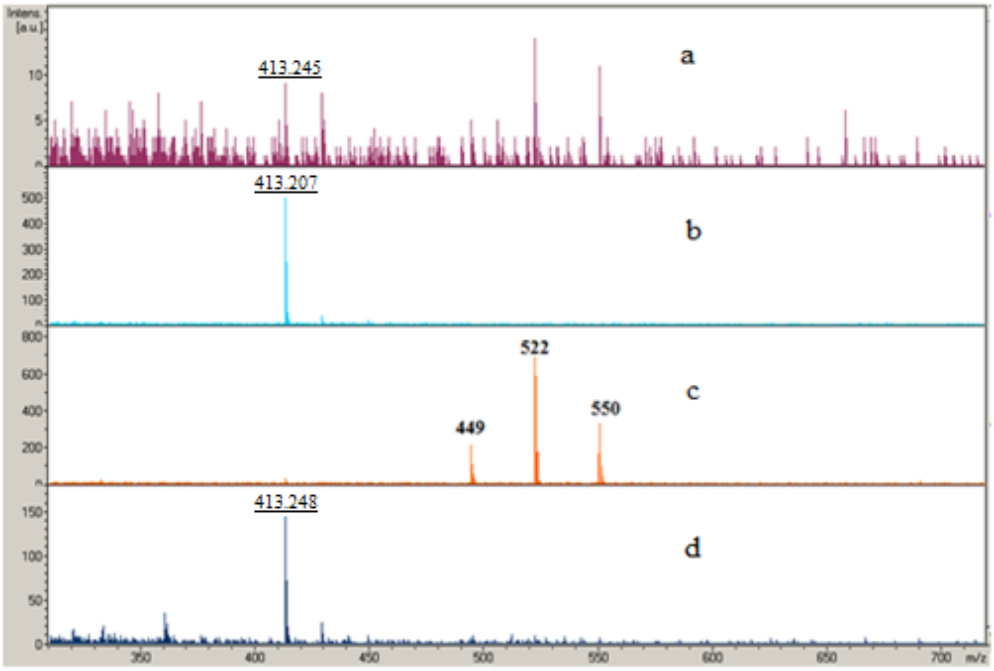

Figure 4. 9 Example of a solvent spotted on a previously checked target cell with different pipettes a) background of spot 1; b) MeOH spotted with Glass pipette; c) background of spot 2; d) MeOH spotted with autopipette

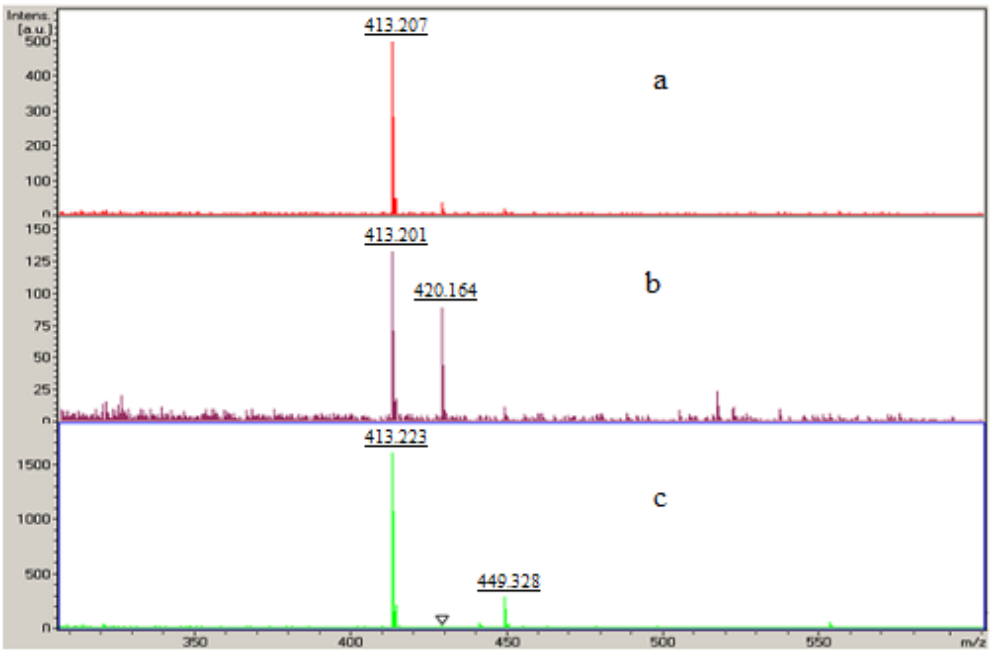

Figure 4. 10 LDI-TOF spectra of solvents tested with glass Pasteur pipette a) MeOH, b) DCM, c) acetone

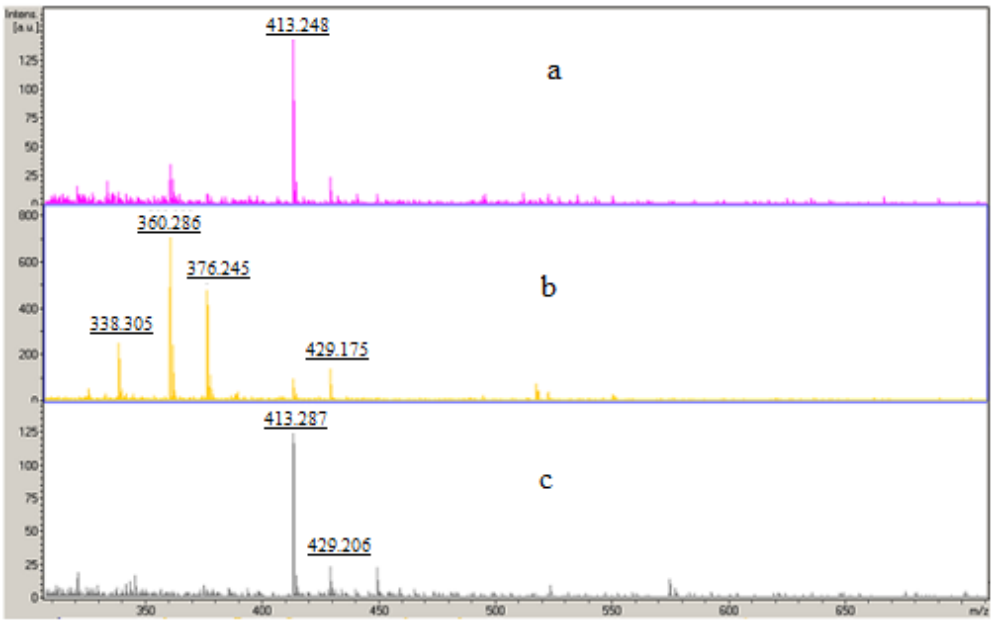

Figure 4. 11 LDI-TOF spectra of solvents tested with Autopipette a) MeOH, b) DCM, c) acetone

In **Figure 4. 11b**, three discrete predominate peaks were observed with *m/z* values 338, 360 and 376. These peaks have been identified as protonated and adduct formation of erucamide, [M+H], [M+Na] and [M+K] respectively. This compound could possibly come from slip agent or detergent.[82] However,

desorption and ionization also afforded an ion *m/z* 465, which is 16 mass unit different from 449. Thus these two ions could also be interpreted as adduct ions with sodium and potassium, which leave it as an unknown contaminant.

These results indicate that di-isooctylphthalate is a major contaminant, which can come from solvents, air,[80] plastic materials used (sample bags, pipette tips and containers) and glass pipette. In this respect sample preparation and handling should be carefully considered to minimize the contamination. It should be noted that all the biochar samples were received in the plastic bags or containers except the sucrose biochars made in house.

4.3.3 Removal or suppression of signal of possible plasticizer using synthetic graphite

Synthetic graphite does not show characteristic biochar ions.[69] A series of experiments were conducted to show if synthetic graphite could absorb plasticizers and reduce their signal. Biochar, graphite, and a mixture of both were soaked in acetone or DCM:MeOH (95:5, v/v) for a period of time. The supernatant from each experiment was analyzed by LDI-TOF.

Spectra (**Figure 4. 12**) showed that the phthalate ion *m/z* 429 was reduced significantly when synthetic graphite was mixed with biochar sample compared to that sample without it, the same trend was also observed when DCM:MeOH solution was used. It was interesting to note that the graphite had only a minor effect on ion *m/z* 701 when acetone was used as a soaking solvent, whereas when DCM:MeOH solution was used, increased intensity of ion *m/z* 701 was observed, **Figure 4. 13**.

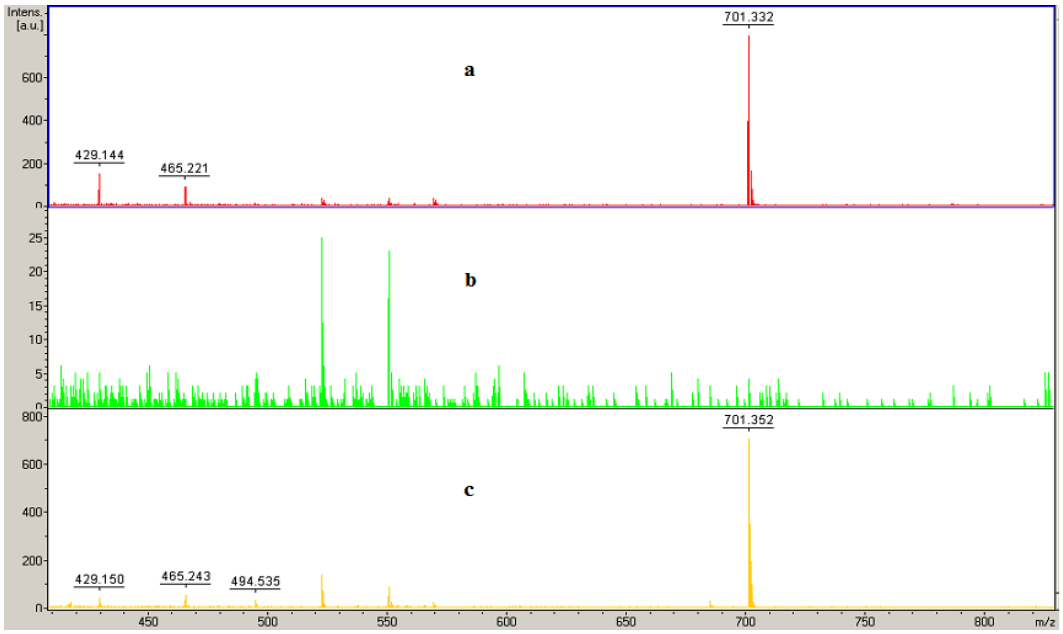

Figure 4. 12 LDI-TOF spectra of plasticizer absorption tests with acetone a) biochar, b) graphite, c) biochar and graphite

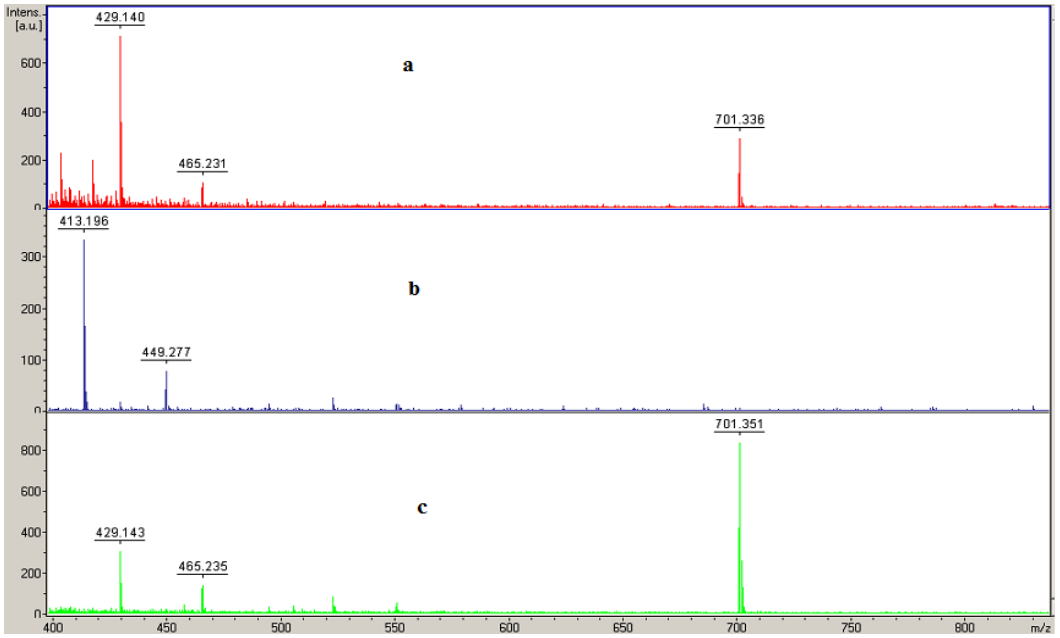

Figure 4. 13 LDI-TOF spectra of plasticizer absorption tests with DCM:MeOH a) biochar, b) graphite, c) both

The results obtained from this experiment indicate that synthetic graphite can be used to minimize ions from phthalate compounds in LDI-TOF of biochar. However, based on the intensity of the peaks obtained from phthalates, it is difficult to make judgments of the quantity in solvents due to the wide variety of sources contributing to the contamination.

Extractives from biochar soluble in non-aqueous solvents

Biochar samples were extracted with a mixed solvent (DCM: MeOH 95:5 v/v) using a Soxhlet extractor for a period of time (19-20 h). The extract was derivatized with Tri-Sil HTP reagent, blow down under a stream of N_2 gas and reconstituted in heptane before being analyzed by GC-MS using full scan mode.

The % w/w of materials extracted from each biochar sample was recorded, **Table 5. 1**. Most of these extractives arise from the condensation of pyrolytic volatiles during cooling, which means that the conditions during carbonization contribute to the amount and type of extractives obtained. **Figure 5. 1** shows the amount of selected extractives for biochars prepared from green waste at different temperatures. The vertical axis is the peak area no adjustment for response has been made; conditions were controlled so that individual injections could be compared. Values are enumerated in **Table 5. 2**.

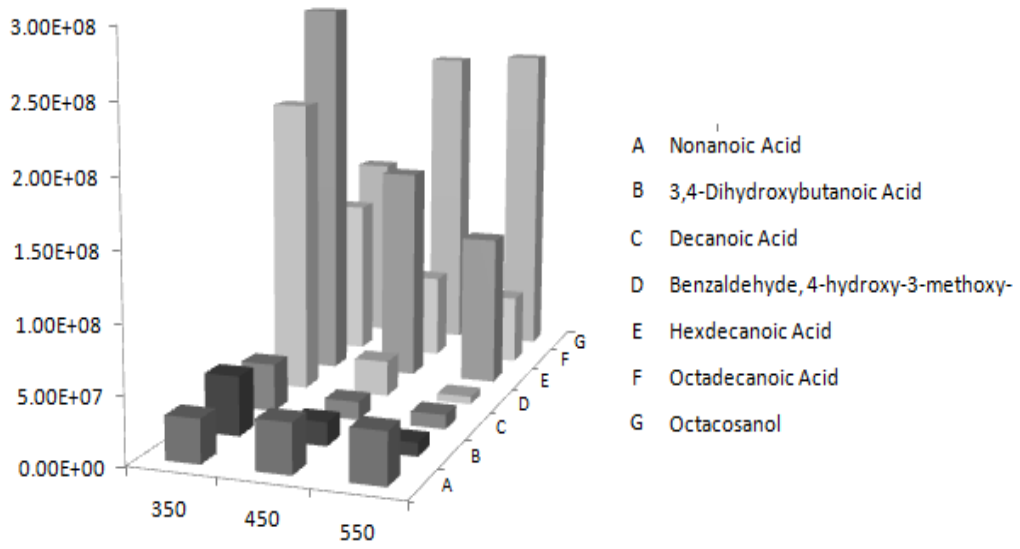

Figure 5. 1 Effect of processing temperature on selected extractives in green waste biochars

Table 5. 1 Weight of dried extractives from various biochars

Sample Name	biochar used (g)	weight of dry extractives (mg)	% w/w of extractive in biochar
Green waste 350 ℃	2.1574	137.00	6.35%
Green waste 450 ℃	2.1548	29.50	1.37%
Green waste 550 ℃	2.1576	20.00	0.93%
Sucrose 400 ℃	0.9837	5.77	0.59%
Sucrose 550 ℃	0.9633	10.73	1.11%
Sucrose 700 ℃	0.9567	29.79	3.11%
Coconut Shell	1.0055	35.30	3.51%
Eucalyptus Sawdust 600 ℃	1.3284	54.80	4.13%
Acacia saligna 400 ℃	1.4792	66.60	4.50%
Hawaii charcoal	1.000	62.60	6.26%

Table 5. 2 Effect of temperature on abundance of selected extractives in green waste biochars prepared with different processing temperatures.

	Peak area[a]		
Name	350˚C	450˚C	550˚C
Nonanoic Acid	3.24E+07	3.68E+07	3.81E+07
3,4-Dihydroxybutanoic Acid	4.42E+07	1.76E+07	1.00E+07
Decanoic Acid	3.56E+07	1.36E+07	1.07E+07
Benzaldehyde, 4-hydroxy-3-methoxy-	2.23E+08	2.71E+07	5.88E+06
Hexdecanoic Acid	2.92E+08	1.63E+08	1.14E+08
Octadecanoic Acid	1.21E+08	6.44E+07	5.29E+07
Octacosanol	1.47E+08	2.43E+08	2.47E+08

[a] No adjustment for response has been made

These results show that % w/w of organic soluble extractives varies with the substrate as well as the conditions used. In the case of green waste (GW) biochar, the total mass decreases as treatment temperature increases presumably because volatiles are degassed to the environment more readily at higher temperatures. The mass of extractives was reflected in their colour, which was darker

(**Figure 5. 2**) and in the aroma, which was stronger at lower temperatures.

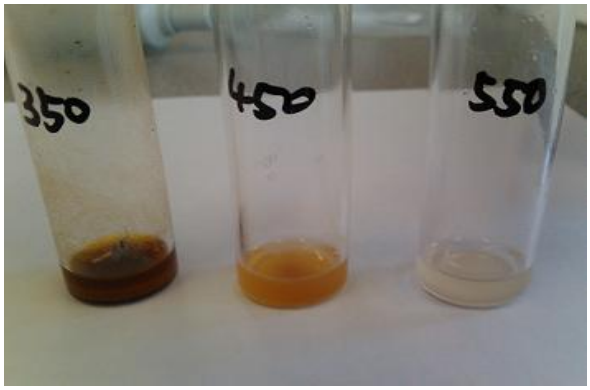

Figure 5. 2 Illustration of the colour of the extracts of green waste biochar made at different temperatures (350-550 ˚C)

It is not appropriate to make direct comparison with sucrose in which this trend is reversed because the sucrose biochars are made from pure crystalline carbohydrate which may well resist decomposition until higher temperatures. Also the sucrose samples were small-scaled and somewhat enclosed which would encourage condensation of volatiles.

Fifty-nine organic compounds have been determined from the biochar samples; compounds were identified by comparison of their mass spectra with the National Institute of Standards (NIST) Mass Spectral Database search. The threshold limit for identification match was set at 50%. These compounds can be separated into groups; the percentage contribution of each group to the total is shown in **Figure 5. 3** for G.W biochar produced at 350 ˚C[*]. These proportions will vary in other biochars, for example **Figure 5. 4** illustrates the percentage contribution in a sucrose biochar which shows reduced aromatics that derive from lignin.

[*] Note that Figure 5.3 shows numbers of compounds in particular groups not mass.

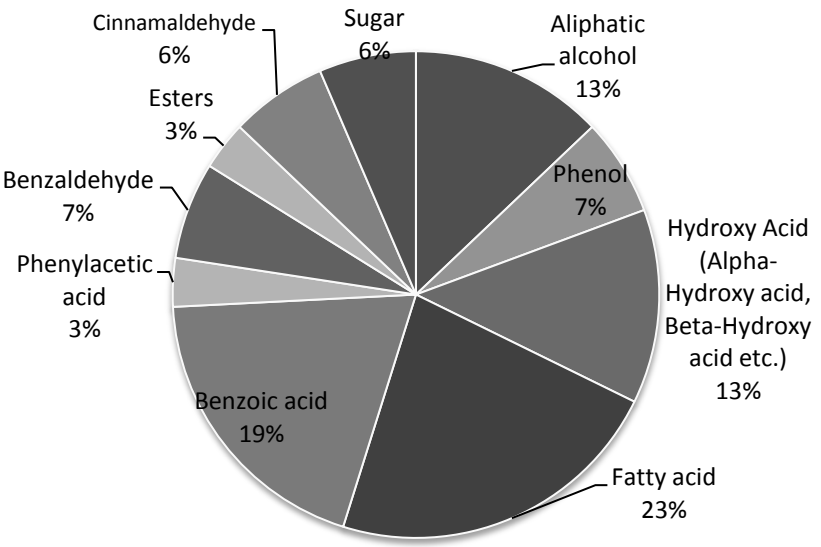

Figure 5. 3 Percentage contribution of compound groups in Green Waste biochar 350˚C

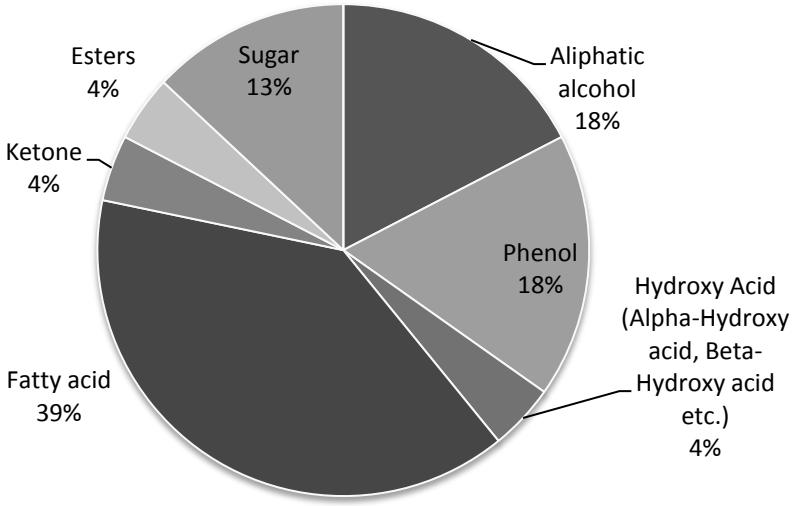

Figure 5. 4 Percentage contribution of compound groups in Sucrose biochar 400 ˚C

Quantitation is difficult because individual compounds will have different responses in the GC-MS. To illustrate this, examples were taken from four groups shown in the figures above and used to determine a response relative to glycerol; these are shown in **Table 5. 3**. This confirms that compounds should be compared only to themselves or with reservations to compounds in the same group.

Table 5. 3 Calculation of the relative ratio of signal response of selected standards to Glycerol

Standard	Relative ratio to Glycerol
Phenol	0.19
Glycerol	1
n-Decanoic Acid	0.05
Syringic Acid	0.01
Lactic acid	0.21

The total ion chromatogram (TIC) of *A.saligna* biochar produced at 400 ˚C is shown in **Figure 5. 6** and **Figure 5. 7** is the TIC of 4-24 minutes expanded. Numbers on the spectra indicate compounds whose identification is shown in the following pages. It should be noted that the mass spectra are of the silylated derivative for example the compound which is eluted at 7.56 minutes which appears as *O*-trimethylsilyphenol is actually phenol in the extract, **Figure 5. 5**.

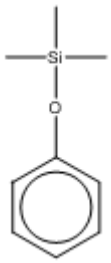

silylated form

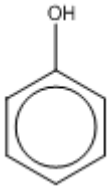

actual compound

Figure 5. 5 Structures of silylated derivative and its original compound

For each peak at a particular retention time the mass spectrum is given above and then underneath is the result of NIST mass spectral database search with a drawing of the silylated compound; the percentage figure is the certainty of the identification. The database does not contain every possible compound and so

may merely be indicating a similarity rather than the absolute identification. The mass spectra of monosaccharides matched extremely poorly with the database search result, due to the similarity of their fragments. Consequently, monosaccharide sugars in the sample were compared with an additional library database, which has built with purchased standards that were analyzed under the same condition. To achieve identification for all the compounds would require purchasing a standard for each and co-injecting them with the unknown; similarly with quantitation, individual standards should be used. This was not done due to the timeframe of this project. The predominant peaks shown in **Figure 5.6** are plasticizers with retention times at 30.129 and 38.216 min, and herbicide (2, 4-D 2-ethylhexyl ester) at 34.794 min.

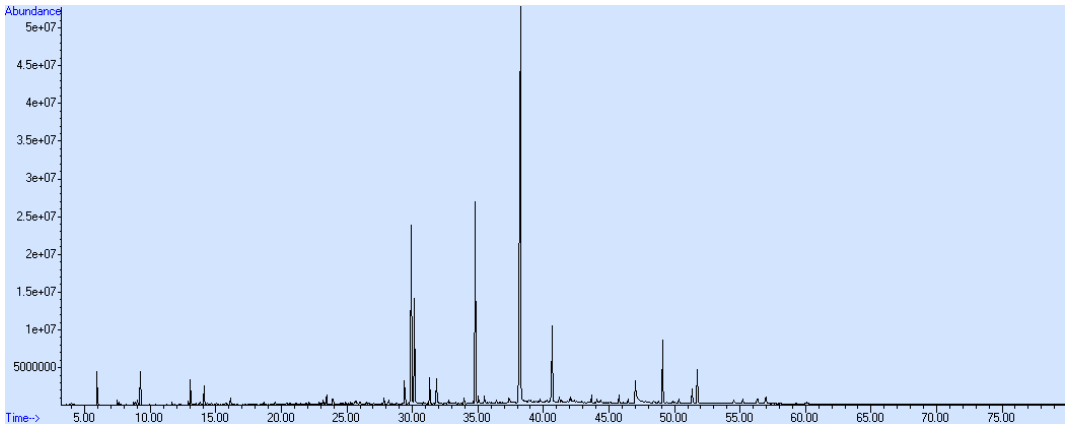

Figure 5. 6 TIC of A. saligna biochar produced at 400 ˚C

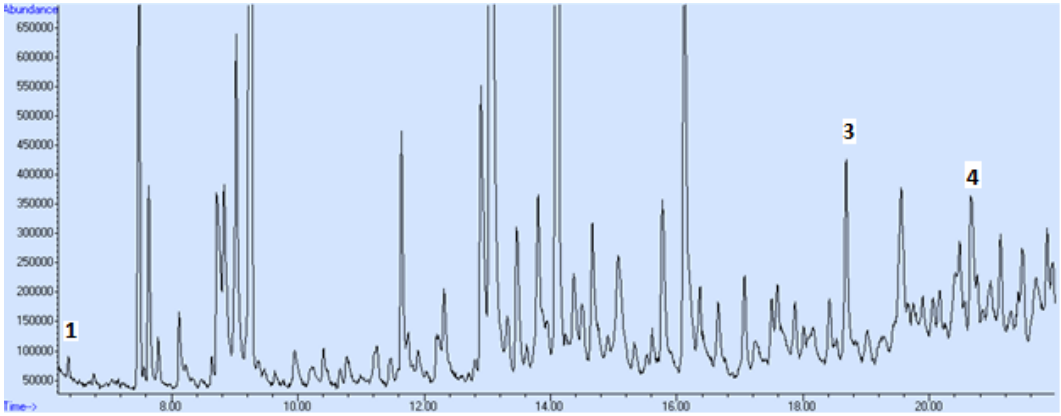

Figure 5. 7 Expanded TIC of A. saligna biochar (400 ˚C) at 4-22 min

The mass spectrum is a representation of the relative concentrations versus *m/z* values. The most intense peak in the spectrum called the base peak, is assigned a value of 100% and the intensities of other fragment peaks are reported as the percentage of the base peak.[83] Some of the peaks in the spectra, such as 207 and 281 amu are well known background peaks from the degradation of a polysiloxane type of column and because the sample solution was silylated, a peak of 73 amu in the mass spectra results from the $Si^{+}(CH_3)_3$ group.

An example of fragmentation identification from different types of compound is described in detail in the following section. The identification of all compounds can be found in the appendix.

1) *1, 2-Propanediol 72.3% match*

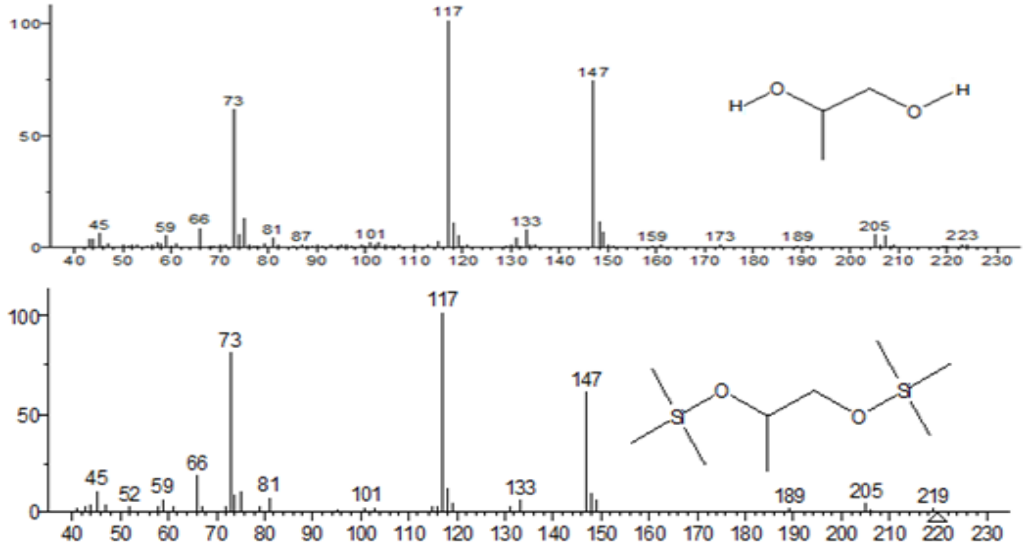

Figure 5. 8 EI mass spectrum of silylated 1, 2-propanediol (6.36 min)

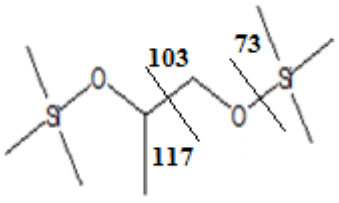

Scheme 5.1 Mass spectral fragmentation of per-*O*-trimethylsilylated 1,2-propanediol

A primary or secondary alcohol usually has a very small molecular ion peak, whereas for a tertiary alcohol it is often undetectable.[83] The molecular ion of this silylated alcohol is not seen. The compound which eluted off the column at 6.36 min is likely to be 1, 2-propanediol (propylene glycol). The presence of a distinct M-15 peak at *m/z* 205 indicates a loss of methyl group from the trimethylsilyl derivative. There are three prominent peaks shown in the mass spectrum **Figure 5. 8**. The ion *m/z* 73 is indicative of $[Si\ (CH_3)_3]^+$ group. The peak at *m/z* 117 is the base peak which resulted from the cleavage of the C-C bond next to the oxygen atom, $[M\text{-}CH_2O\text{-}\ Si\ (CH_3)_3]^+$. The ion $Me_3Si\text{-}O^+ = SiMe_2$ at *m/z* 147 is the characteristic peak of a *cis*-hydroxylated trimethylsilyl derivative.[84] The illustration of fragmentation is shown above (**Scheme 5.1**).

2) *<u>Guaiacol</u> 97% match (seen only in 350 ˚C GW and so not marked on the sample chromatogram)*

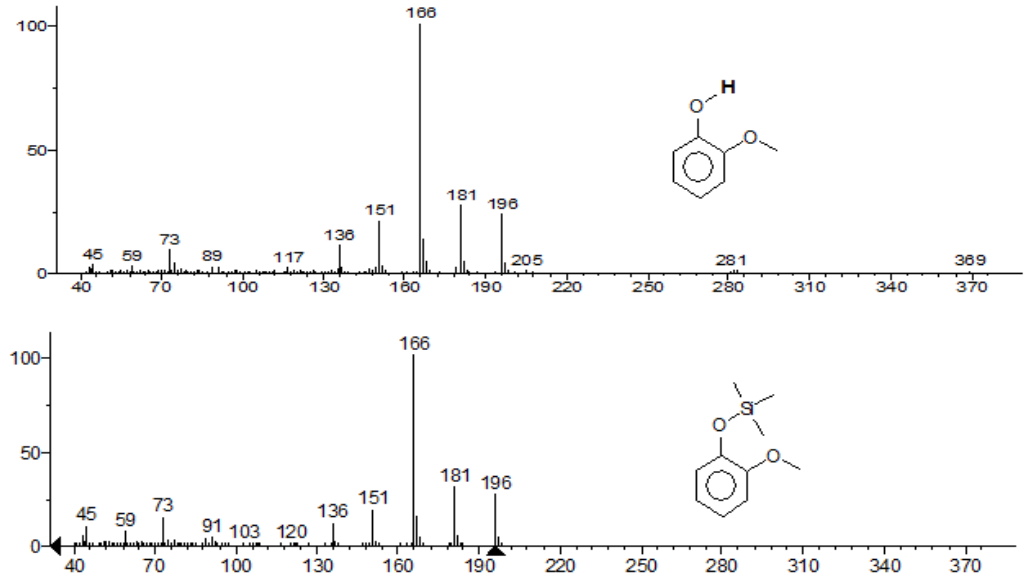

Figure 5. 9 Mass spectrum of silylated Guaiacol (12.37 min)

Guaiacol (2-methoxyphenol) is also found in wood smoke,[85] and probably resulted from the pyrolysis of lignin. The compound contributes to the flavour of many compounds, such as roasted coffee.[86] The major fragments shown in the spectra correspond to a series of losses of a methyl group, and the presence of a

conspicuous molecular ion peak identifies an aromatic ring. The identification of guaiacol is relatively high, and it was found only in green waste biochar that was made at 350 ˚C, suggesting it can be easily decomposed or volatilized at higher temperature.

3) *Decanoic acid* *84% match*

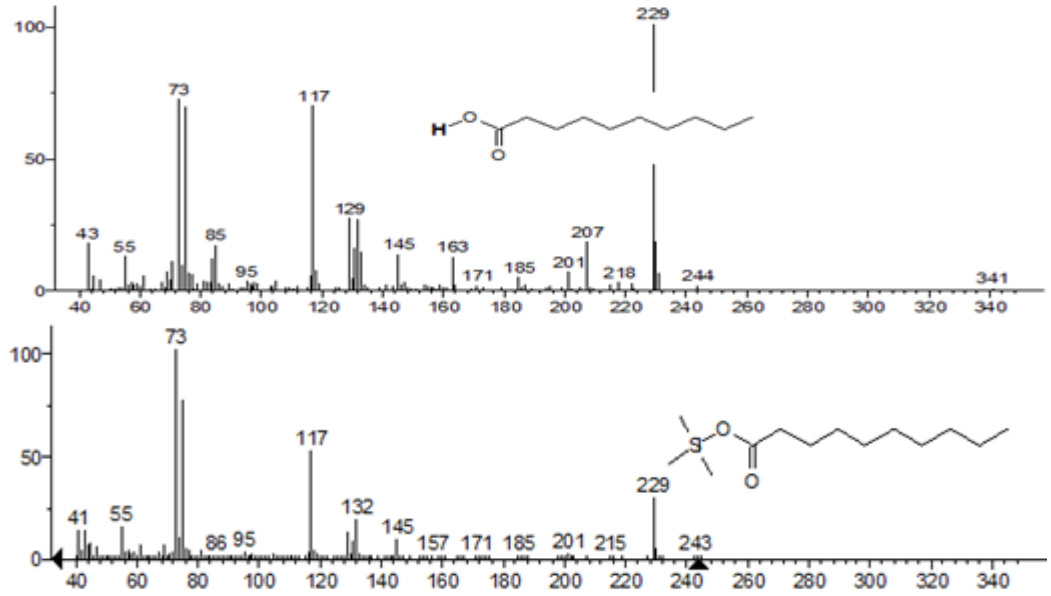

Figure 5. 10 EI mass spectrum of silylated decanoic acid (18.69 min)

The molecular ion peak is usually weak for straight chain monocarboxylic acid but discernible[83] as shown in both spectra at *m/z* 244 (**Figure 5. 10**). The predominant peak at *m/z* 229 is a distinct M-15 peak from the loss of a methyl from the trimethylsilyl group. The presence of ions *m/z* 132 and 117 are the characteristic peaks of carboxylic acids resulting from the McLafferty rearrangement[83] (**Scheme 5.2**) and α cleavage of a C-C bond next to C=O respectively. The spectrum contains peaks indicating cleavage of a C-C bond with charge on the alkyl fragment (*m/z* 43, 85) or on the oxygen-containing fragment (*m/z* 117, 131, 145), **Scheme 5.3**. The other interesting feature of the spectrum is the presence of an intense peak at *m/z* 75 together with *m/z* 73. This ion pair is

also observed in all other fatty acids that present in the sample, thus they may be considered as a characteristic ion pair for silylated fatty acids.

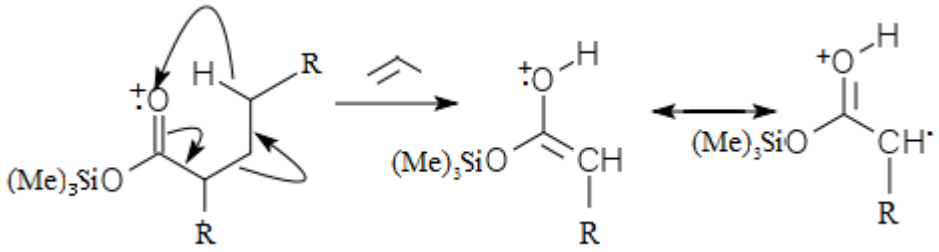

Scheme 5.2 McLafferty rearrangement[83] of per-*O*-trimethylsilylated decanoic acid

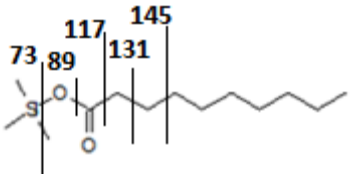

Schematic 5.3 Mass spectral fragmentation of per-*O*-trimethylsilylated decanoic acid

4) *<u>4-hydroxy-3-methoxy-benzaldehyde</u>* *87% match*

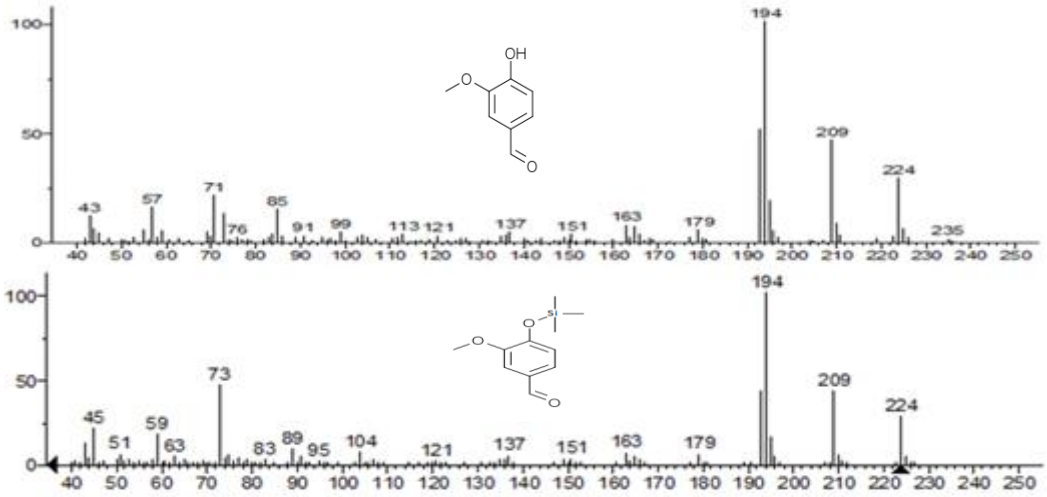

Figure 5. 11 EI mass spectrum of silylated 4-hydroxy-3-methoxy-benzaldehyde (20.69 min)

The molecular ion is a conspicuous peak observed at *m/z* 224, **Figure 5. 11**. A series of peaks are observed at *m/z* 179, 194 and 209 from the successive loss of methyl from the trimethylsilyl group as for the other aromatic compound, methoxyphenol described previously.

Figure 5. 13 shows an expansion of the TIC from 22-53 minutes the numbered peaks are discussed below.

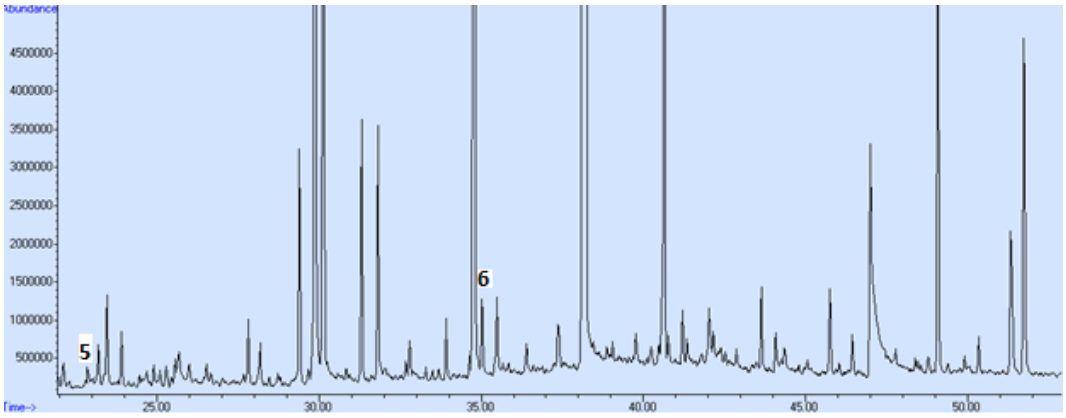

Figure 5. 13 Expanded TIC of A. saligna biochar 400 ˚C at 22-53 min

5) *<u>Benzophenone</u>* *78% match*

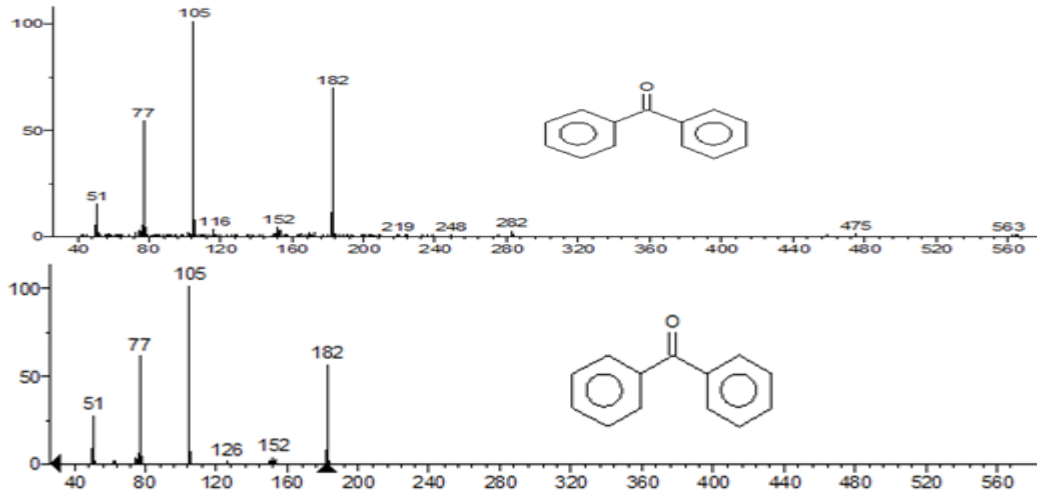

Figure 5. 12 EI mass spectra of benzophenone (22.86 min)

The molecular ion peak of an aromatic ketone is usually prominent due to stabilization by the aromatic ring in the molecule. The base peak at *m/z* 105 is characteristic of a resonance stabilized acylium ion fragment. The loss of CO from the acylium ion results in the fragment ion *m/z* 77, the aryl ion.[83] This compound was found only in *A. saligna* 400˚C biochar extracts.

6) *Triclopyr 2-butoxyethyl ester* *99% match*

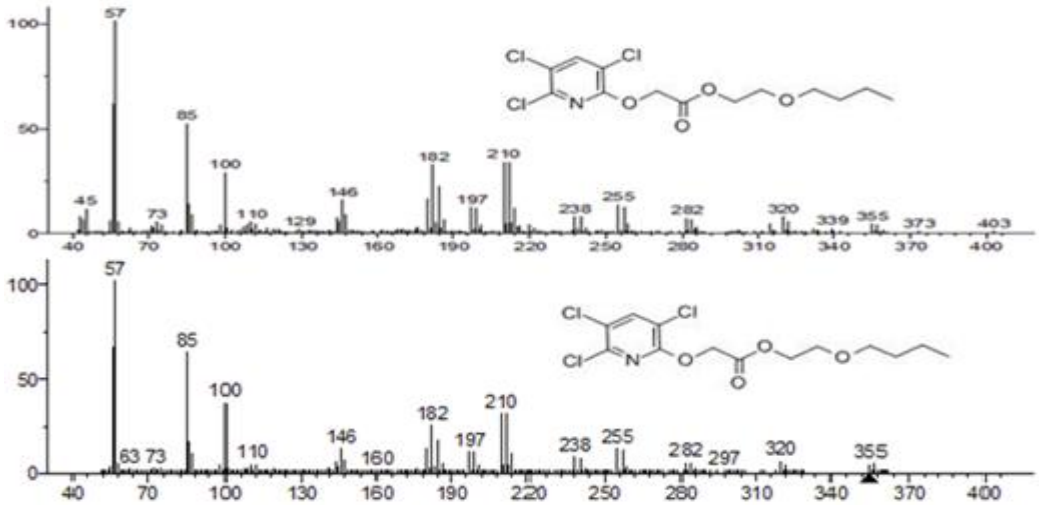

Figure 5. 14 EI mass spectrum of triclopyr 2-butoxyethyl ester (35.03 min)

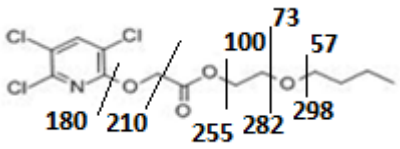

Scheme 5.4 Mass spectral fragmentation of triclopyr 2-butoxyethyl ester

Triclopyr 2-butoxyethyl ester is a common commercial herbicide which is used to control woody and broadleaf plants by affecting hormone behaviour in the plant thus causing uncontrollable growth or death.[87] The molecular ion peak is observable. Cleavage of the C-O bond on the side chain resulted in the base peak at *m/z* 57, **Scheme 5.4**. The characteristic isotope pattern of a chlorine containing compound is observed with multiple ion groupings for example the fragment m/z

180 in **Scheme 5.4** actually shows predominantly 182 with 184 (~30%) and 186 (~3%). This compound was found only in the *A. saligna* (400 ˚C) sample. Since *A. saligna* is regarded as a weed in much of southern and south eastern Australia it is possible that this herbicide has been used as a control agent.[88]

All fifty-nine compounds observed with the exception of sugars and open chain alkanes are shown in **Table 5. 4** together with significant ions from the mass spectrum; compounds that are marked in this table were also found in the study carried out by Schnitzer *et al.* (2006) [89] using curie-point pyrolysis-gas chromatography mass spectrometry (Cp Py-GC-MS). In this study, all the N-heterocyclic compounds that were identified by Py-GC-MS are not observed, because the nitrogen content in chicken manure is more than in normal biochars, and secondly the Py-GC-MS analysis is a different process to that used here. Straight chain alkanes are listed separately in **Table 5.5**, the compounds that were observed by Py-GC-MS are also marked. Because the spectra of these are often very similar the % matches are not as good as those in **Table 5. 4**. Sugars are listed in **Table 5. 6**, not all sugars were observed in all the biochars. Arabinopyranose and glucopyranose were observed in all biochars, although arabinofuranose was only seen in biochar made from sucrose at 700 ˚C, and xylopyranose was present in all biochars as well with the exception of biochars made from green waste. A large signal with m/z 217 is characteristic of furanose sugars whereas *m/z* 204 is characteristic of pyranose sugars.

Table 5. 5 List of straight chain alkanes found in biochars

RT	Name	Cross-reference with Py-GC-MS data[89]	Molecular formula	Molecular weight
7.64	Dodecane	√	$C_{12}H_{26}$	170
13.804	2,6,11-trimethyl dodecane		$C_{15}H_{32}$	212
14.371	Tridecane	√	$C_{13}H_{28}$	184
17.073	Tetradecane	√	$C_{14}H_{30}$	198
26.683	Octadecane		$C_{18}H_{37}$	254
30.835	Icosane		$C_{20}H_{42}$	282
36.395	Tricosane		$C_{23}H_{48}$	324
39.757	Pentacosane		$C_{25}H_{52}$	352
41.349	Hexacosane		$C_{26}H_{54}$	366

Table 5. 4 Organic compounds determined in biochar as their per-*O*-trimethylsilyl derivatives

RT	Name	Cross-referencing with Py-GC-MS data[89]	Molecular formula	Molecular weight	Significant ions in mass spectrum (Base peak in bold)
6.363	1,2-Propanediol (propylene glycol)		$C_3H_8O_2$	76	73,**117**,147
7.557	Phenol	√	C_6H_5OH	94	**151**, 166
7.940	Lactic Acid (2-hydroxypropanoic Acid)		$C_3H_6O_3$	90	73, 117, **147**, 191, 219
8.125	Hexanoic Acid		$C_6H_{12}O_2$	116	75, 117, 131, **173**
8.314	Glycolic Acid		$C_2H_4O_3$	76	73, **147**, 177, 205
8.462	1,3-Butanediol		$C_4H_{10}O_2$	90	73, 103, 117, 129, **147**
9.638	2-methylphenol	√	C_7H_8O	108	91, 135, 149,**165**, 180
9.953	3-mehtylphenol	√	C_7H_8O	108	**165**, 180
10.217	3-Hydroxypropanoic Acid		$C_3H_6O_3$	90	73, **147**, 177, 219
10.481	Hydroxycarbamic acid		CH_3NO_3	77	**73**, **147**, 278
12.317	3,5-Dimethylphenol		$C_8H_{10}O$	122	105, **170**, 194
12.367	2-methoxyphenol	√	$C_7H_8O_2$	124	136, 151, **166**, 181, 196

RT	Name	Cross-referencing with Py-GC-MS data[89]	Molecular formula	Molecular weight	Significant ions in mass spectrum (Base peak in bold)
12.810	4-Hydroxybutanoic Acid		$C_4H_8O_3$	104	73, 117, **147**, 233
12.946	Benzoic Acid		$C_7H_6O_2$	122	77, 105, 135, **179**, 194
13.063	Diethylene Glycol		$C_4H_{10}O_3$	106	**73**, 117, 147
13.475	Octanoic Acid		$C_8H_{16}O_2$	144	73, 117, **201**
13.819	2,3-Butanediol		$C_4H_{10}O_2$	90	73, **117**, 147
14.110	Glycerol		$C_3H_8O_3$	92	**73**,147, 205, 218
14.750	2,2-dihydroxyacetic acid		$C_2H_4O_4$	92	73, 147,**191**
15.765	2-Methylbenzoic Acid		$C_8H_8O_2$	189	91, 119, 149, **193**, 208
16.134	Nonanoic Acid		$C_9H_{18}O_2$	158	73,117,215
16.986	2,3-Dimethoxyphenylacetic acid		$C_{10}H_{12}O_4$	196	**73,** 179, 194, 253, 268
17.602	2,2-dihydroxyacetic acid		$C_2H_4O_4$	92	**73**,147, 205, 218
18.41	3,4-Dihydroxybutanoic Acid		$C_4H_8O_4$	120	**73**, 147, 189,233, 321
18.691	Decanoic Acid		$C_{10}H_{20}O_2$	172	73, 117, **229**

RT	Name	Cross-referencing with Py-GC-MS data[89]	Molecular formula	Molecular weight	Significant ions in mass spectrum (Base peak in bold)
20.059	Hexanedioic acid		$C_6H_{10}O_4$	146	73, 111, 147, 275
20.686	Benzaldehyde, 4-hydroxy-3-methoxy-		$C_8H_8O_3$	152	**194**, 209, 224
21.301	2-Naphthol		$C_{10}H_8O$	144	**201**, 216
21.849	3-Methoxycinnamic Acid		$C_{10}H_{10}O_3$	178	**161**, 191, 235, 250
22.856	Benzophenone		$C_{13}H_{10}O$	182	52, 77, **105**, 182
22.927	4-Hydroxybenzoic Acid		$C_7H_6O_3$	138	73, 193, 223, **267**, 282
23.458	Dodecanoic Acid		$C_{12}H_{24}O_2$	200	73, 117, **257**
24.667	3,5-Dimethoxy-4-hydroxybenzaldehyde		$C_9H_{10}O_4$	182	**224**, 239, 254
25.685	*n*-Tridecanoic acid		$C_{13}H_{26}O_2$	214	**73**, 117, 129, 271
26.126	Vanillic acid (4-Hydroxy-3-methoxybenzoic acid)		$C_8H_8O_4$	168	193, 223, 253, 267,**297,** 312
27.43	Protocatechuic acid(3,4-dihydroxybenzoic Acid)		$C_7H_6O_4$	154	73, **193**, 355, 370
27.668	Monocaprylin		$C_{11}H_{22}O_4$	218	57, 73, 127, 147, **259**

RT	Name	Cross-referencing with Py-GC-MS data[89]	Molecular formula	Molecular weight	Significant ions in mass spectrum (Base peak in bold)
27.757	4-hydroxy-3-methoxycinnamaldehyde		$C_{10}H_{10}O_3$	178	192, **220**, 235, 250
27.812	Tetradecanoic Acid		$C_{14}H_{28}O_2$	228	73, 117, 132, **285**
27.996	2-hydroxy-2-(4-hydroxy-3-methoxyphenyl)acetic acid		$C_9H_{10}O_5$	198	73, **297**
29.089	Syringic acid (3,5-Dimethoxy-4-hydroxybenzoic acid)		$C_9H_{10}O_5$	198	223, 253, 297, 312, **327**, 342
30.478	Gallic Acid(3,4,5-trihydroxybenzoic Acid)		$C_7H_6O_5$	170	73, 281, 443, **458**
31.113	4-Hydroxy-3,5-dimethoxycinnamaldehyde		$C_{11}H_{13}O_4$	208	73,**222**, 250, 265, 280
31.814	Hexdecanoic Acid		$C_{16}H_{32}O_2$	256	73,117, 132,145, **313**
33.679	Heptadecanoic Acid		$C_{17}H_{34}O_2$	270	73, 117, 129, 145, **327**
34.794	2,4-D, ethylhexyl ester		$C_{16}H_{22}C_{l2}O_3$	333	43, 57, 71, **220**, 332
35.026	Triclopyr butoxyethyl ester(BEE)		$C_{13}H_{16}C_{l3}NO_4$	356	**57**, 85, 100, 182, 210
35.485	Octadecanoic Acid		$C_{18}H_{36}O_2$	284	73, 117,132, 145, **341**, 356
38.228	Hexanedioic Acid, bis(2-ethylhexyl)ester		$C_{22}H_{42}O_4$	370	57, 70, 112, **129**, 147

RT	Name	Cross-referencing with Py-GC-MS data[89]	Molecular formula	Molecular weight	Significant ions in mass spectrum (Base peak in bold)
38.875	Eicosanoic acid		$C_{20}H_{40}O_2$	312	73, 117, 132, 145, **369**, 384
40.119	1,2-benzenedicarboxylic acid,dicyclohexyl ester		$C_{20}H_{26}O_4$	330	**149**, 167
42.022	Docosanoic Acid		$C_{22}H_{44}O_2$	340	73, 117, 132, 145, **397**, 412
43.008	Sucrose		$C_{12}H_{22}O_{11}$	342	73, 217, **361**, 437, 451
43.644	Tricosanoic Acid		$C_{23}H_{46}O_2$	354	75, **411**
46.054	2-Heptacosanone		$C_{27}H_{54}O$	394	**59**, 71, 85, 96, 394
49.096	Octacosanol		$C_{28}H_{58}O$	410	75, **467**

Table 5. 6 Sugars observed in biochars, identified by co-elution with a standard

RT[a]	Name	Molecular weight	Significant ions in mass spectrum
23.185, 23.898	Arabinose	150	73, 147, 191, 204, **217** (pyranose)
24.547			73, 147, **217** (furanose)
25.275, 26.513	Xylose	150	73, 147, 191,**204**, 217
29.439, 31.302	Glucose	180	73, 147, 191,**204**, 217

[a] Multiple retention times due to α and β forms of the pyranose

Studies of specialty biochars or extracts from various suppliers

6.1 Introduction

In this chapter the studies carried out on different biochar samples obtained from two suppliers will be discussed. Biochar samples that were obtained from Stephen Joseph (University of New South Wales, Sydney, Australia) can be divided into four groups based on their source, BMC*, paper sludge, chicken manure and wood biochars (*Acacia saligna* and *Eucalyptus*). All of the BMC samples are made from about 30% biochar, 30% chicken manure and 10% minerals. The biochar content derives from *A.*saligna biochar or from Jarrah hardwood charcoal; the minerals are from clays which were obtained from Geraldton in Northern WA or from Southern WA. All of the biochars had different processing temperatures. The LDI-TOF results of these samples showed the biochar characteristic peaks described by Bourke *et al.*[69] An interesting feature of the spectra is the relative enrichment of ion *m/z* 701, which is known to be the pseudomolecular ion with potassium $[M+K]^+$; this varies between samples, probably due to the difference in mineral composition of the biochars.

The sample from Massey University was an extract from a pine biochar which was produced from pine wood chips as feedstock. The feedstock was pyrolyzed at 550 ˚C after drying in a 60 ˚C oven. The biochar was extracted three times using a solvent mixture comprised of acetone: MeOH: water (20:4:3) to remove the volatile fraction. Massey University who had discovered that pre-extraction improved microbial growth, were interested in finding out what compounds were present that might inhibit the bacterial growth.

* BMC stands for Biochar mineral complex

6.2 Analysis of biochar supplied from the University of New South Wales

All of these samples were digested and analyzed by ICP-MS. The results for the elements present in greater than trace amount (Na; Mg; Al; P; K; Ca; Fe and Mn) are given in **Table 6. 1**. In paper, cellulose pulp is the major component which derived from wood. The high concentration of various ions in paper sludge biochar could have been added during the pulping or as inks or binders post pulping. These results showed a very clear difference between the BMC biochars and the wood biochars, there are similarities between the paper sludge biochar and the BMC's except for the potassium content which is similar to the biochar made from chicken litter. The sodium and potassium concentration determined in the biochars by ICP-MS had a good correlation with the intensity of pseudo molecular ions observed in LDI-TOF analysis. For example, paper sludge biochar, which has a higher concentration of sodium compared to potassium ion gave a high intensity of ion *m/z* 685 compared to 701 in the LDI-TOF spectrum.

BMC 7/09 biochar was analyzed by laser ablation ICP-MS to determine if there was any obvious difference between outer and inner layers. Two of the larger particles were cut into four sections each and analyzed. There were some technical difficulties as the pellets partially disintegrated upon cutting. In **Figure 6. 1**, there is obviously some differences but no clear trend is observed. This may be due to the problems with cutting or due to an uneven distribution in the manufacture of the pellets.

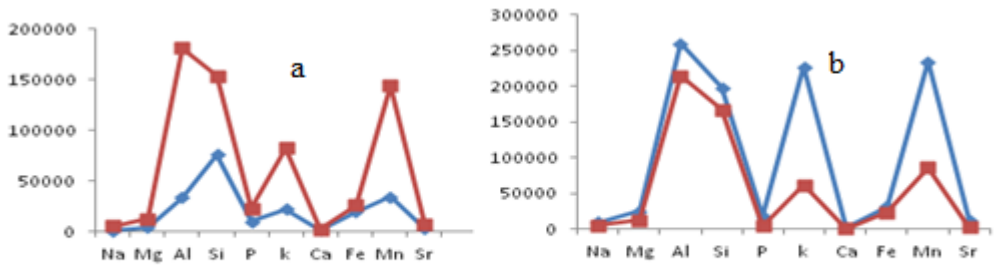

Figure 6.1 The elemental analysis of outer (□) and inner (◇) layer of two BMC 7/09 particles (a) and (b)

Table 6. 1 Concentration (ppb) of the major elements in biochar samples

	Na 23	**Mg 24**	**Al 27**	**P 31**	**K 39**	**Ca 43**	**Fe 54**	**Mn 55**
BMC 3/09	2505.95	10735.01	10959.80	10735.01	6196.15	21118.10	14465.98	1544.40
BMC 5/09	1697.39	17420.73	11434.56	17420.73	6585.69	31358.72	13169.68	7739.40
BMC 6/09	1581.67	29276.33	16938.22	29276.33	11214.07	40649.13	13606.79	2884.73
BMC 7/09	1468.76	34472.17	14785.50	34472.17	11644.27	50659.51	11737.42	5637.14
A. saligna Biochar 400˚C	1359.89	417.07	173.07	417.07	8945.14	7093.87	74.78	11.12
Eucalyptus Sawdust 550˚C	347.90	79.53	835.86	79.53	383.08	3474.28	1578.30	24.49
Eucalyptus Sawdust 600˚C	293.26	15.62	194.25	15.62	316.28	159.77	997.89	10.51
Chicken litter 450˚C	620.11	132.80	2073.37	132.80	899.01	1139.35	9328.14	124.62
Paper Sludge 550˚C	1865.43	1475.51	18178.65	1475.51	825.01	47993.24	5808.33	227.20

6.3 Analysis of extractives from pine biochar supplied from Massey University

The three organic extract samples were evaporated to dryness using reduced pressure (40 ˚C) and the weight of the residue was recorded, **Table 6. 2**.

Table 6. 2 Weight of dried extracts

Sample label	Weight of dry residue (mg)
Extract #1	278.3
Extract #2	27.7
Extract #3	3.2

Silylation of the dry residue of extract #1 without the internal standard was trialled to ensure that the standard did not correspond to any prominent peaks, **Figure 6. 2**. Secondly, the experiment was repeated with the internal standard added, **Figure 6. 3**. There were concerns that the usual method, in which the silylating fluid is removed by evaporation, could cause loss of small volatile molecules. Therefore the final method injected the silylating mixture directly, **Figure 6. 4**. Analysis was only carried out on extract #1 on the basis that the three are probably the same, although proportions may differ.

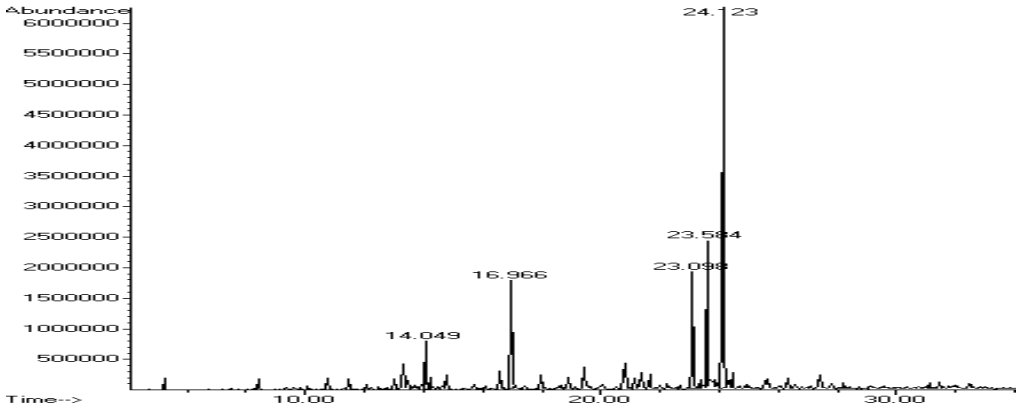

Figure 6. 2 Total Ion Chromatogram (TIC) of 2.21 mg dry substance of extract #1 analysed without Mannitol internal standard with blow down and re-dissolving in heptane

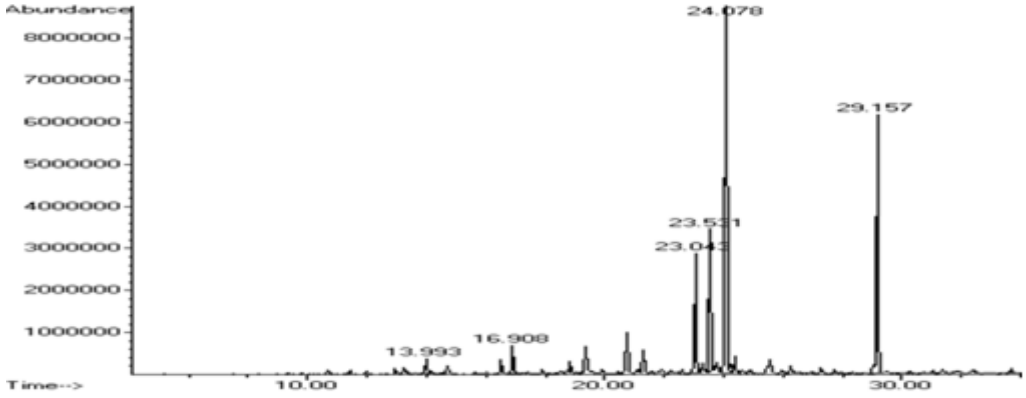

Figure 6. 3 TIC of dry substance of extract #1 with Mannitol (29.157 min) as internal standard with blow down and re-dissolving in heptane

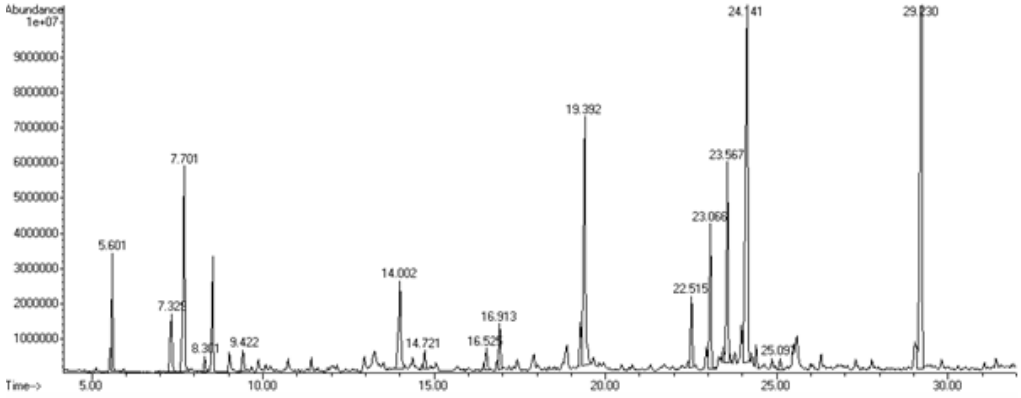

Figure 6. 4 TIC of 1.72 mg dry substance of extract #1 with Mannitol without blow down and injected directly

Table 6. 3 Masses of analytes observed in GC of dried extracts

RT[a]	Compound	Ratio[b] (Analyte/IS)	Analyte (mg)
5.601	1,2-ethanediol	0.1142	0.0064
5.943	2-hydroxypropanol	0.0691	0.0039
6.987	phenol	0.0024	0.0001
7.329	2-hydroxypropanoic acid	0.1129	0.0063
7.701	acetic acid	0.2627	0.0147
8.301	Silylating fluid	0.0184	0.001
8.527	Silylating fluid	0.1507	0.0084
9.422	3-hydroxypropanoic acid	0.0401	0.0022
10.732	3-methyl-1-hydroxycyclohexene	0.0218	0.0012
11.408	1,2-ethanediol	0.0187	0.001
12.963	2,3-dihydroxydioxane	0.0374	0.0021
13.259	2,5-dihydroxydioxane	1.2899	0.0722
14.002	2-hydroxyphenol	0.203	0.0114
14.374	2-methylbutanedioic acid	0.014	0.0008

RT[a]	Compound	Ratio[b] (Analyte/IS)	Analyte (mg)
15.061	methylmaleic acid	0.0156	0.0009
16.525	sugar	0.0474	0.0027
16.913	trihydroxypentane	0.0875	0.0049
19.392	trihydroxypentane	0.55	0.0308
21.317	pentose sugar	0.3108	0.0174
22.515	2-hydroxyhexanedioic acid	0.1073	0.006
23.066	levoglucosanfuranose	0.2273	0.0127
23.567	anhydrohexopyranose	0.3163	0.0177
24.141	levoglucosan	0.8863	0.0496
26.289	3-vanilpropanol	0.0235	0.0013

[a]RT = retention time [b] response factor assumed to be 1

The values in **Table 6. 3** are taken from the chromatogram shown in **Figure 6. 4**. The major substances present appear to be derived from sugars, the biggest peak is almost certainly levoglucosan[90] (1, 6-anhydroglucopyranose) and it is possible that there is a similar anhydrosugar of another hexose. The identification of levoglucosanfuranose is similarly confident. These results are different to those obtained with the solvent mixture (DCM: MeOH) used in this study principally by the dominant presence of anhydrosugars which are often the major fraction of water soluble organic compounds that derived from the thermal decomposition of cellulose[97]. The pyrolysis process can be controlled to produce a high yield of levoglucosan in terms of the initial cellulose content.[90- 92] The pine biochar produced by Massey contains 39.7% of cellulose. Some microbes can utilize levoglucosan as an energy source.[93] The data obtained from GC-MS showed that there are some phenol and substituted phenol compounds such as vanilpropanol, which probably derive from lignin and to which might be attributed the inhibition of microbial growth property.[90] A study of aqueous extracts from pine needles performed by Feng *et al.* (2010)[95] suggested that the organic acids content effectively inhibited some bacterial growth. The relative ratio of signal response of organic acids to glycerol is very small (refer to **Table 5.3**), which means that there are probably more organic acids present than the mass indicated in **Table 5.3**.

A lack of mass balance between the amount detected by GC-MS and the initial input amount of materials was noted. The dry substance from extract #1 (~2 mg)

was dissolved in MeOH and analyzed together with common matrix including: SDHB, HCCA and dithranol on MALDI-TOF, where the MeOH solution was also introduced in ESI-MS. The results obtained from these analyses showed no significant higher molecular weight material from the dry substance.

ICP-MS was used to determine the inorganic content. The total percentage of cations (0.43%) that have been extracted from the pine biochar showed (**Table 6. 4**) comparability with the total difference of cations in the pine biochar before and after solvent extraction that were analyzed by Hill Laboratories. The total difference of cations from Hill's results is 1572 mg/kg which is equivalent to 0.1572 g/100 g or 0.1572% which is approximately three times smaller than the value calculated in **Table 6.4**, but at least in the same order of magnitude which is acceptable considering the diverse approaches used. The results showed that the cations which gave the biggest difference between the biochars tested are also the predominant cations observed in the residue. However the results obtained are still unable to resolve the mass balance issue and no toxic element was detected in amounts that would be thought to be the cause of inhibition of microbial growth.

High performance liquid chromatography was carried out to detect oligosaccharides that are unlikely to be detected by GC-MS; the information obtained from this technique gave a general indication of some higher sugars such as tetra- or pentasaccharides but was unable to resolve the mass balance issue. Probably the most significant cause of failure to get mass balance is lack of appropriate response factors.

Table 6. 4 Mineral composition analyzed via ICP-MS and calculated total percentage of cations that have been extracted from pine biochar

	B 10	**Na 23**	**Mg 24**	**Al 27**	**Si 28**	**P 31**	**K 39**	**Ca 43**	**V 51**	**Cr 52**	**Fe 54**	**Mn 55**	**Co 59**	**Ni 60**	**Cu 65**	**Zn 68**	**Se 82**	**Sr 88**	**Ba 137**	**Hg 202**
Charcoal sample	10.2	1919.9	224.9	258.7	33.9	38.6	7647.2	4561.4	0.3	35.1	237.8	66.5	0.4	5.3	4.2	34.8	0.2	4.4	4.0	0.1
Procedural blank	5.5			60.8	3.1	28.7	-150.0	-1.0			109.1	20.0			-0.1	0.6	0.0	0.3	0.0	-0.4
Actual µg/L	5	1920	225	198	31	10	7797	4562	0	35	129	47	0	5	4	34	0	4	4	0
µg in total residue	1.4	549.9	64.4	56.7	8.8	2.8	2233.3	1306.8	0.1	10.0	36.9	13.3	0.1	1.5	1.2	9.8	0.1	1.2	1.1	0.1
Cations (g)/ biochar (g) %	1.36 E-04	5.50 E-02	6.44 E-03	5.67 E-03	8.80 E-04	2.81 E-04	2.23 E-01	1.31 E-01	7.39 E-06	1.00 E-03	3.69 E-03	1.33 E-03	1.12 E-05	1.53 E-04	1.25 E-04	9.78 E-04	6.19 E-06	1.19 E-04	1.14 E-04	1.26 E-05
Total % w/w extracted cations in biochar	**0.43%**																			

An example of calculation % w/w using potassium (K) ion:

Total residue extracted from biochar = 309.2 mg

The concentration of digested solution = 1079.5 mg/L

Amount of K in solution = 7797 μg/L

Therefore the mass (μg) of cations in total residue:

$$7797 \times \frac{309.2}{1079.5} = 2233.3 \ (\mu g)$$

That is the mass of extracted cations in 1 g of biochar, 2233.3 μg/g

So the total % by mass (g) of cations extracted from 1g of biochar equals

$$2233.3/10^6 \times 100 = 0.223\% \approx 0.2\%$$

Conclusions and further work

7.1 Summary of results

1) Acetone was the best solvent for ion *m/z* 701determination using LDI-TOF analysis with a rapid method. It also can be used as a soaking solvent for extracting the ion *m/z* 701 into supernatant for analysis by ESI-TOF.

2) The adduct ion experiment carried out by LDI-TOF determined that the ion pair *m/z* 685 and 701 are ion $[M+Na]^+$ and $[M+K]^+$ respectively, of which give mass difference of 16. Thus actual molecular mass for the ion pair is 662 (molecule X). The other thought to be characteristic peaks of biochar, 317, 429, 453 and 465 are also behaved in the same way.

3) Results from the LDI-TOF of biochar spiked with fullerene indicates that peak *m/z* 701 observed in biochar is not a fragment ion of fullerene.

4) Results from NMR experiments carried out on the biochar sample either in liquid form or in solid form suggested that it contains multiple highly aromatic compounds and possibly some aliphatic carbons or adsorbed contaminant.

5) A water extract of biochar sample was analyzed by LC-MS with a APCI source using direct infusion method, a series of fragment ions of *m/z* 663, $[M+H]^+$; including *m/z* 607, 531 and 495 was observed. The mass difference between these fragments is 56 amu which suggests a polymeric structure. This water extract has also introduced via HPLC using a C18 column, the elution time of ion *m/z* 663 is at 9.6 minutes with 80% MeOH used as mobile phase. However the ease of fragmentation of the ion *m/z* 663in aqueous solvent is unlike the observations in LDI-TOF, thus the ion observed in both techniques is possibly not the same ion.

6) The molecular formulas of ion pair *m/z* 685 and 701 were determined by high resolution ESI-TOF, $C_{49}H_{58}$**Na**O and $C_{49}H_{58}$**K**O respectively. The only difference between the two formulas is the adduct ion, thus the molecular formula of *m/z* 662 is $C_{49}H_{58}O$. The same technique has also been applied to

the determination of other believed characteristic ions of biochar. The results show that these ions are probably from plasticizers.

7) Blank tests were performed to determine the possible contamination source. Results showed that defined contaminants could come from the solvent, pipette and/or even the air due to the ability of biochar to absorb organic compounds.

8) The presumed plasticizer signals could be suppressed in LDI-TOF by mixing with synthetic graphite but *m/z* 701 was not suppressed.

9) LA-ICP-MS data obtained from the ablation of outer and inner side of a biochar with large particle size showed no distinguishable difference between the two sides. Technical difficulties in cutting the pellets could affect the results.

10) Results from elemental analysis of digested biochar samples performed by ICP-MS showed a very clear difference between the biochars made from mineral complex and the simple wood biochars. It also showed that the sample which contained more sodium ion than potassium then it gave a high intensity of peak *m/z* 685 in comparison with peak *m/z* 701 in LDI-TOF spectrum.

11) Tri-Sil HTP resulted in better GC-MS chromatogram of extractives than TMSI.

12) Fifty-nine compounds were identified in extracts from various biochars analyzed by GC-MS.

13) The mass of extractable material decreases with increasing processing temperature in some commercial biochars.

14) Extractable material from sucrose biochars lacks many of the phenolics that are present in plant based biochars confirming that these phenolics derive from lignin.

15) Different extraction solvents give different ranges of compounds.

7.2 Future work

In this study, several extraction methods have been used to extract the molecule X. With the soaking protocol, a carbon cluster region was formed during the process which suppressed the peak of the molecule X in the LDI-TOF analysis, whereas the soxhlet extraction method was capable of providing a reliable LDI-TOF spectrum with less effect of the carbon clusters. The problem of this method is that it is a time and solvent consuming protocol. Another issue of these extraction methods is the loss of molecule X during evaporation process either under reduced pressure in a rotovap or when blowing down with N_2 gas. All of these suggested that more development should be carried out on investigating a suitable extraction method of this molecule X from biochar, so that more investigation of the structure can be made, for example by NMR.

More detailed work needs to be carried out so that more accurate quantitation of extractives can occur, for example calculation of appropriate response factors.

Since different solvents give different compounds future extractions should use a range of solvents of differing polarity to ensure all extractives are solubilized. The biochar can be extracted with polar to non-polar solvents such as water, methanol, isopropanol, chloroform, ethyl acetate and hexane. The residue of each one of the extractions should be analyzed in succession and the elemental analysis which also includes CHO, N, S should be carried out on the biochar before and after the extractions to determine the polarity of the extractable compounds.

References

1. Lehmann, J.; Joseph, S., *Biochar for environmental management :science and technology*. Earthscan: London ;Sterling, VA, 2009; p 416.

2. Lehmann, J.; Gaunt, J.; Rondon, M., Bio-char sequestration in terrestrial ecosystems-a review. *Mitigation and Adaptation Strategies for Global Change* **2006,** *11*, 403-427.

3. Schmidt, M. W. I.; Noack, A. G., Black carbon in soils and sediments: Analysis, distribution, implications, and current challenges. *Global Biogeochemical Cycles* **2000,** *14*, 777-794.

4. Neves, E. G.; Bartone, R. N.; Petersen, J. B.; Heckenberger, M. J., The timing of Terra Preta formation in the central Amazon: Archaeological data from three sites. In *Amazonian dark earths: explorations in space and time*, Glaser, B.; Woods, W. I., Eds. Springer: New York, 2004; pp 125-134.

5. Wood, I. W.; Teixeira, G. W.; Lehmann, J.; Steiner, C.; WinklerPrins, A.; Rebellato, L., Amazonian dark earths: Wim Sombroek's vision. Springer: Berlin, 2009. (accessed 02/09/2011).

6. Talberg, A. The basics of biochar. http://www.aph.gov.au/library/pubs/bn/sci/Biochar.htm (accessed December, 2011).

7. Tryon, E. H., Effect of charcoal on certain physical, chemical, and biological properties of forest soils. *Ecological Monographs* **1948,** *18*, 81-115.

8. Retan, G. A., Charcoal as a means of solving some nursery problems. *Forestry Quarterly* **1915,** *13*, 25-30.

9. Scott, E. L.; van Haveren, J.; Sanders, J. P. M., The production of chemicals in biobased economy. In *The biobased economy: biofuels, materials and chemicals in the post-oil era*, Langeveld, H.; Sanders, J.; Meeusen, M., Eds. Earthscan: UK, 2010; pp 146-153.

10. Antal, M. J.; Grønli, M., The art, science, and technology of charcoal production. *Industrial & Engineering Chemistry Research.* **2003,** *42* (8), 1619-1640.

11. Patterson, W. A.; Edwards, K. J.; Maguire, D. J., Microscopic charcoal as a fossil indicator of fire. *Quaternary Science Reviews* **1987,** *6* (1), 3-23.

12. Stassen, H. E., Developments in charcoal production technology. In *Wood energy*, FO, Ed. FAO (Food and Agriculture Organization United Nations): Italy, 2002; Vol. 53.

13. Goley, G. *Charcoal making in developing countries*; Technical Report No.5; IIED: London, 1986; pp 124-129.

14. Antal, M. J.; Mok, W. S. L.; Varhegyi, G.; Szekely, T., Review of methods for improving the yield of charcoal from biomass. *Energy Fuels* **1990,** *4* (3), 221-225.

15. Steierer, F. Highlights on wood charcoal: 2004-2009. http://faostat.fao.org/Portals/_Faostat/documents/pdf/Wood%20charcoal.pdf (accessed 5-09-2011).

16. Shafizadeh, F., Chemistry of pyrolysis and combusion of wood. *Progress in Biomass Conversion* **1982,** *3*, 51-76.

17. Van Zwieten, L.; Kimber, S.; Morris, S.; Downie, A.; Berger, E.; Rust, J.; Scheer, C., Influence of biochars on flux of N_2O and CO_2 from ferrosol. *Australian Journal of Soil Research* **2010,** *48* (7), 555-568.

18. Bridgwater, T., IEA Bioenergy 27th update: Biomass pyrolysis. *Biomass and Bioenergy* **2007,** *31* (4), VII-XVIII.

19. Mohan, D.; Pittman, J.; C. U.; Steele, P. H., Pyrolysis of wood/biomass for bio-oil: A critical review. *Energy Fuels* **2006,** *20*, 848-889.

20. Boaterng, A. A., Characterization and thermal conversion of charcoal derived from fluidized-bed fast pyrolysis oil prodction of switchgrass. *Industrial & Engineering Chemistry Research.* **2007,** *46*, 8857-8862.

21. Brewer, E. C.; Schmidt-Rohr, K.; Satrio, A. J.; Brown, C. R., Characterization of biochar from fast pyrolysis and gasification systems. *Environmental Progress & Sustainable Energy* **2009,** *28* (3), 386-396.

22. Bruun, E. W. Application of fast pyrolysis biochar to a loamy soil http://130.226.56.153/rispubl/reports/ris-phd-78.pdf (accessed 6/09/2011).

23. Bridgwater, A. V., *An introduction to fast pyrolysis of biomass for fuels and chemicals*. CPL Scientific Publishing Services Ltd: Newbury, UK, 1999.

24. Vassilev, S.; Baxter, D.; Andersen, L.; Vassileva, C., An overiew of the chemical composition of biomass. *Fuel* **2010,** *89* (5), 913-933.

25. Chandrakant, P.; Bisaria, V. S., Simultaneous bioconversion of cellulose and hemicellulose to ethanol. *Critical Reviews in Biotechnology* **1998,** *18*, 295-331.

26. de Vrije, T.; de Haas, G. G.; Tan, G. B.; Keijsers, E. R. P.; Caassem, P. A. M., Pretreatment of miscanthus for hydrogen production by Thermotoga elfii. *International journal of Hydrogen Energy* **2002,** *27*, 1381-1390.

27. Sassner, P.; Galbe, M.; Zacchi, G., Bioethanol production based on simultaneous saccharification and fermentation of steam-pretreated Salix at high dry matter content. *Enzyme and Microbial Technology* **2006,** *39*, 756-762.

28. Hamelinck, C. N.; van Hooijidonk, G.; Faaij, A., Ethanol from lignocellulosic biomass: Techno-economic performance in short-middle and long-term. *Biomass and Bioenergy* **2005,** *28*, 384-410.

29. McMurry, J., Fundamental of organic chemistry. In *Biomolecules: Carbohydrates*, Seventh ed.; Mary Finch: CA, USA, 2010; p 491.

30. Sjostrom, E., *Wood Chemistry: foundamentals and applications*. second ed.; Academic Press: 1993.

31. Sun, R. C.; Tomkinson, J.; Ma, P. L.; Liang, S. F., Comparative study of hemicelluloses from rice straw by alkali and hydrogen peroxide treatments. *Carbohydrate Polymers* **2000,** *42* (2), 111-122.

32. Antal, M. J., Effects of reactor severity on the gas-phase pyrolysis of cellulose- and kraft lignin-derived volatile matter. *Industrial & Engineering Chemistry Process Design and Development* **1983,** *22*, 366.

33. Sjostrom, E., Wood chemistry - fundamentals and applications. *Academic Press:1981* **1981**, 223.

34. Sarkanen, K. V.; Ludwig, C. H., Lignins occurrence, formation, structure and reactions. *Journal of Polymer Science* **1972,** *10* (3), 228-230.

35. Lignin. http://www.pnas.org/content/103/42/15497/F1.expansion.html (accessed 04-12-2011).

36. Sluiter, A.; Ruiz, R.; Scarlata, C.; Sluiter, J.; Templeton, D. *Determination of extractives in biomass*; Technical Report: NREL/TP-510-42619; Midwest Research Institute: Colorado, 2005.

37. Jenkins, B. M.; Bakker, R. R.; Wei, J. B., On the properties of washed straw. *Biomass and Bioenergy* **1996,** *10* (4), 177-200.

38. Jinno, D.; Gupta, A. K.; Yoshikawa, K., Determination of chemical kinetic parameters of surrogate solid wastes. *Journal of Engineering for Gas Turbines and Power* **2004,** *126* (4), 685-692.

39. Williams, P. T.; Besler, S., The influence of temperature and heating rate on the slow pyrolysis of biomass. *Renewable Energy* **1996,** *7*, 223-250.

40. Yang, H.; Yan, R.; Chen, H.; Lee, D. H.; Zheng, C., Characteristics of hemicellulose, cellulose and lignin pyrolysis. *Fuel* **2007,** *86*, 1781-1788.

41. Rutherford, D. W.; Wershaw, R. L.; Cox, L. G. *Changes in composition and porosity occurring during the thermal degradation of wood and wood components*; United States Geological Survey: Reston, VA, 2004.

42. Randall, J. T.; Bernal, J. D., The diffraction of X-rays and electrons by amorphous solids, liquids, and gases. *Journal of Physical Chemistry* **1934,** *39* (9), 1249.

43. Walker Jr, P. L.; Seeley, S. B. In *Fine grinding of Ceylon natural graphite*, Proceedings of the Third Biennial Carbon Conference, Buffalo, NY, Pergamon Press: Buffalo, NY, 1957; pp 481-494.

44. Aylmore, L. A. G.; Quirk, J. P., Domain or Turbostratic Structure of Clays. *Nature* **1960,** *187* (4742), 1046-1048.

45. Franklin, R. E. In *Crystallite growth in graphitizing and non-graphitizing carbons*, Proceedings of the Royal Society of London, series A, mathematical and physical science, 1951; pp 196-218.

46. Emmerich, F. G.; Luengo, C. A., Babassu charcoal: a sulfurless renewable thermo-reducing feedstock for steelmaking. *Biomass and Bioenergy* **1996,** *10*, 41-44.

47. Setton, R.; Bernier, P.; Lefrant, S., *Carbon molecules and materials*. CRC Press: Boca Raton, FL, 2002.

48. Polyaniline Nanoporous Carbon Electrode Materials Yield Most Powerful Supercapacitors to Date Say Max Planck Researchers. http://nanopatentsandinnovations.blogspot.co.nz/2010/01/polyaniline-nanoporous-carbon-electrode.html (accessed January, 2012).

49. Ishimaru, K.; Vystavel, T.; Bronsveld, P.; Hata, T.; Imamura, Y.; Hosson, K. D., Diamond and pore structure observed in wood charcoal. *Journal of Wood Science* **2001,** *47*, 414-416.

50. Kurosaki, F.; Ishimaru, K.; Hata, T.; Bronsveld, P.; Kobayashi, E.; Imamura, Y., Microstructure of wood charcoal prepared by flash heating. *Carbon* **2003,** *41*, 3057-3062.

51. Harris, P. J. F., Structure of non-graphitizing carbons. *International Materials Reviews* **1997,** *42* (5), 206-218.

52. Marsh, H.; Rodriguez-Reinoso, F., *Activated Carbon*. Elsevier Ltd.: UK, 2006.

53. Gray, E.; Marsh, H.; Robertson, J., Physical characteristics of charcoal for use in gunpowder. *Journal of Materials Science* **1985,** *20*, 597-611.

54. Lua, A. C.; Yang, T.; Guo, J., Effects of pyrolysis conditions on the properties of activated carbons prepared from pistachio-nut shells. *Journal of Analytical and Applied Pyrolysis* **2004,** *72*, 279-287.

55. Postor-Villegas, J.; Valenzuela-Calahorro, C.; Bernalte-Garcia, A.; Gomez-Serrano, V., Characterization study of char and activated carbon prepared from raw and extracted rockrose. *Carbon* **1993,** *31*, 1061-1069.

56. Laine, J.; Simoni, S.; Calles, R., Preparation of activated carbon from coconut shell in a small scale concurrent flow rotary kiln. *Chemical Engineering Communications* **1991,** *99*, 15-23.

57. Wildman, J.; Derbyshire, F., Origins and functions of macroporosity of activated carbons from coal and wood precursors. *Fuel* **1991,** *70*, 655-661.

58. Biagini, E.; Tognotti, L. In *Characterization of biomass chars*, Proceedings of the Seventh International Conference on Energy for Clean Environment, Lisbon, Portugal, Lisbon, Portugal, 2003.

59. Rodriguez-Miraso, J.; Cordero, T.; Rodriguez, J. J., Preparation and characterization of activated carbons from eucalyptus kraft lignin. *Carbon* **1993,** *31*, 87-95.

60. Aygun, A.; Yenisoy-Karakas, S.; Duman, I., Production of granular activated carbon from fruit stones and nutshells and evaluation of their physical, chemical and adsorption properties. *Microporous and Mesoporous Materials* **2003,** *66*, 189-195.

61. Cetin, E.; Moghtaderi, B.; Gupta, R.; Wall, T. F., Influence of pyrolysis conditions on the structure and gasification reactivity of biomass chars. *Fuel* **2004,** *83*, 2139-2150.

62. Brown, R. A.; Kercher, A. K.; Nguyen, T. H.; Nagle, D. C.; Ball, W. P., Production and characterization of synthetic wood chars for use as surrogates for natural sorbents. *Organic Geochemistry* **2006,** *37*, 321-333.

63. Bourke, J. Preparation and properties of natural, demineralized, pure, and doped carbons from biomass; model of the chemical structure of carbonized charcoal. MSc, University of Waikato, Hamilton, 2006.

64. Guo, J.; Lua, A. C., Characterization of chars pyrolyzed from oil palm stones for the preparation of activated carbons. *Journal of Analytical and Applied Pyrolysis* **1998,** *46*, 113-125.

65. Przybilla, L.; Brand, J.-D.; Yoshimura, K.; Räder, H. J.; Müllen, K., MALDI-TOF Mass spectrometry of insoluble giant polycyclic aromatic hydrocarbons by a new method of sample preparation. *Analytical Chemistry* **2000,** *72* (19), 4591-4597.

66. Edwards, W. F.; Jin, L.; Thies, M. C., MALDI-TOF mass spectrometry: Obtaining reliable mass spectra for insoluble carbonaceous pitches. *Carbon* **2003,** *41* (14), 2761-2768.

67. Sedo, O.; Alberti, M.; Janca, J.; Havel, J., Laser desorption-ionization time of flight mass spectrometry of various carbon materials. *Carbon* **2006,** *44* (5), 840-847.

68. Grainger, M. Categorisation and discrimination of automotive glass fragments by laser ablation inductively coupled plasma mass-spectrometry (LA-ICP-MS) for forensic purposes. MSc Thesis, University of Waikato, Hamilton, 2010.

69. Bourke, J.; Manley-Harris, M.; Fushimi, C.; Dowaki, K.; Nunoura, T.; Antal, M. J., Do all carbonized charcoals have the same chemical structure? 2. A

model of the chemical structure of carbonized charcoal. *Industrial & Engineering Chemistry Research* **2007,** *46* (18), 5954-5967.

70. Suckau, D.; Resemann, A.; Schuerenberg, M.; Hufnagel, P.; Franzen, J.; Holle, A., A novel MALDI LIFT-TOF/TOF mass spectrometer for proteomics. *Analytical and Bioanalytical Chemistry* **2003,** *376*, 952-965.

71. Westman-Brinkmalm, A.; Brinkmalm, G., A mass spectrometer's building blocks. In *Mass spectrometry instrumentation, interpretation, and applications*, Ekman Rolf; Silberring Jerzy; Westman-Brinkmalm Ann; Agnieszka, K., Eds. John Wiley & Sons, Inc.: Hoboken, New Jersey, 2009; pp 15-70.

72. Wilkins, L. C.; O. Lay, J., Jackson, *Identification of microorganisms by mass spectrometry*. John Wiley & Sons, Inc.: Hoboken, New Jersey, 2006; p 49.

73. Roepstorff, P., MALDI-TOF mass spectrometry in protein chemistry. In *Proteomics in functional genomics*, Jolles, P.; Jornvall, H., Eds. Birkhauser Verlag: Basel, Switzerland, 2000.

74. Apicella, B.; Ciajolo, A.; Millan, M.; Galmes, C.; Herod, A. A.; Kandiyoti, R., Oligomeric carbon and siloxane series observed by matrix-assisted laser desorption/ionisation and laser desorption/ionisation mass spectrometry during the analysis of soot formed in fuel-rich flames. *Rapid Communications in Mass Spectrometry* **2004,** *18* (3), 331-338.

75. Cadogan, D. F.; Howick, C. J., Plasticizers. In *Kirk-Othmer Encyclopedia of Chemical Technology*, John Wiley & Sons, Inc.: 2000.

76. Mersiowsky, I.; Weller, M.; Ejlertsson, J., Fate of Plasticised PVC Products under Landfill Conditions: A Laboratory-Scale Landfill Simulation Reactor Study. *Water Research* **2001,** *35* (13), 3063-3070.

77. Fromme, H.; Kuchler, T.; Otto, T.; Pilz, K.; Muller, J.; Wenzel, A., Occurrence of phthalates and bisphenol A and F in the environment. *Water Research* **2002,** *36* (6), 1429-1438.

78. Keller, B. O.; Sui, J.; Young, A. B.; Whittal, R. M., Interferences and contaminants encountered in modern mass spectrometry. *Analytica Chimica Acta* **2008,** *627* (1), 71-81.

79. Ghisari, M.; Bonefeld-Jorgensen, E. C., Effects of plasticizers and their mixtures on estrogen receptor and thyroid hormone functions. *Toxicology Letters* **2009,** *189* (1), 67-77.

80. Otake, T.; Toshinaga, J.; Yanagisawa, Y., Analysis of organic esters of plasticizer in indoor air by GC-MS and GC-FPD. *Environmental Science and Technology* **2001,** *35*, 3099-3102.

81. Paez, A.; Howe, A., Skin deep. *Canadian Chemical News* 2004, p 14.

82. Chen, J.; Li, J.; Hu, T.; Walther, B., Fundamental study of erucamide used as a slip agent. *Journal of Vaccum Science and Technology A* **2007,** *25*, 886.

83. Silverstein, R. M.; Webster, F. X.; Kiemle, D. J., *Spectrometric identification of organic compounds*. Seventh ed.; John Wiley & Sons, Inc.: Hoboken, USA, 2005.

84. Lonngren, J.; Svensson, S., Mass spectometery in structural analysis of natural carbonhydrates. *Advances* **1974,** *29*, 48.

85. Leslle, A. E.; Geoffrey, N. R., Analysis of condensates from wood smoke: components dericed from polysaccharides and lignins. *Environmental Science and Technology* **1991,** *25* (6), 1133-1147.

86. Dorfner, R.; Ferge, T.; Kettrup, A.; Zimmermann, R.; Yeretzian, C., Real-Time Monitoring of 4-Vinylguaiacol, Guaiacol, and Phenol during Coffee Roasting by Resonant Laser Ionization Time-of-Flight Mass Spectrometry. *Journal of Agricultural and Food Chemistry* **2003,** *51* (19), 5768-5773.

87. Begley, P.; Foulger, B. E., Detection of trace levels of triclopyr using capillary gas chromatography—electron-capture negative-ion chemical ionization mass spectrometry. *Journal of Chromatography A* **1988,** *438* (0), 45-53.

88. Randall, R. P., *A global compendium of weeds*. R.G. & F. J.: Melbourne, 2002.

89. Schnitzer, M. I.; Monreal, C. M.; Jandl, G.; Leinweber, P.; Fransham, P. B., The conversion of chicken manure to biooil by fast pyrolysis II. Analysis of chicken manure, biooils, char by curie-point pyrolysis- gas chromatography/ mass spectometry. *Journal of Environmental Science and Health Part B* **2006,** *42*, 79-95.

90. Prosen, E. M.; Radlein, D.; Piskorz, J.; Scott, D. S.; Legge, R. L., Microbial utilization of levoglucosan in wood pyrolysate as a carbon and energy source. *Biotechnology and Bioengineering* **1993,** *42* (4), 538-541.

91. Lomax, J. A.; Boon, J. J.; Hoffman, R. A., Characterization of polysaccharides by in-source pyrolysis positive and negative ion dirrect chemical ionisation mass spectrometry. *Carbohydrate Research* **1991,** *221*, 219-233.

92. Piskorz, J.; Radlein, D.; Scott, D. S.; Czernik, S., Pretreatment of wood and cellulose for production of sugars by fast pyrolysis. *Journal of Analytical and Applied Pyrolysis* **1989,** *16*, 127-136.

93. Kitamura, Y.; Yasui, T., Purification and some properties of levoglucosan (1,6-anhydro-b-D-glucopyranose) kinase from the yeast. *Agricultural and Biological Chemistry* **1991,** *55* (2), 523-529.

94. Joseph, S., Extraction and analysis of biochar-associated organic compounds. Sydney, 2011.

95. Feng, S.; Zeng, W.; Luo, f.; Zhao, j.; Yang, z.; Sun, q., Antibacterial activity of organic acids in aqueous extracts from pine needles (*Pinus massoniana* Lamb.). *Food Science and Biotechnology* **2010,** *19* (1), 35-41.

96. Turn, S. Q.; Kinoshita, C. M.; Ishimura, D. M., Removal of inorganic constitutents of biomass feedstocks by mechanical dewatering and leaching. *Biomass and Bioenergy* **1997,** *12* (4), 241-252.

97 Simoneit, B. R. T.; Elias, V. O.; Kobayashi, M.; Kawamura, K.; Rushdi, A. I.; Medeiros, P. M.; Rogge, W. F.; Didyk, B. M., Sugars dominant water-soluble organic compounds in soils and characterization as tracers in atmospheric particulate matter. *Environmental Science & Technology* **2004,** *38* (22), 5939-5949.

Appendix 1

A Model structure of biochar

The initial work was done and counted towards an assignment in CHEM 502-10Y Physical Chemistry.

From the previous computational study of the model structures of molecule X, results showed that the putative structures for $C_{49}H_{58}O$ are less stable than $C_{38}H_{62}O_9$ due to the high total energy calculated with B3lyp the most widely used method in density functional theory (DFT). However, structures of $C_{49}H_{58}O$ have a higher unsaturation value, the indication of high aromaticity which is to be expected. The two most stable structures for formula $C_{49}H_{58}O$ have some degree of similarity as shown in **Figure 9.1**. The cleavage of the C-C bonds next to the heteroatom could result in the loss a C_3H_4O group, and the delocalization of bonds within the aromatic rings able to form a stable ion. The C_3H_4O group has a mass of 56 amu which agrees with the fragments' mass difference of molecule X obtained from LC-MS analyses. But this cleavage of C-C bond only able to explain one of the loss of 56 not the 2nd loss of 56. This is merely a preliminary study, an investigation of the isotope ratio of the molecule X should be carried out. The calculated fullerene $^{12}C/^{13}C$ isotopic values can then be used as a reference to predict the number of carbons in this molecule. To help with its structural modelling; this may requires a development of separation/purification method of this compound from biochar.

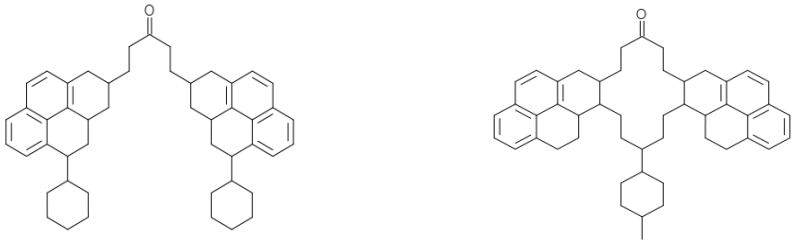

8 9

Figure 9.1 *The most stable 2D and 3D structures for $C_{49}H_{58}O$*